Nuclear Physics B314 (1989) 467–518
North-Holland, Amsterdam

THE GROSS–NEVEU MODEL AND THE PSEUDOFERMION ALGORITHM

Massimo CAMPOSTRINI, Giuseppe CURCI and Paolo ROSSI

Dipartimento di Fisica dell'Università and I.N.F.N., I-56100 Pisa, Italy

Received 1 February 1988
(Revised 8 August 1988)

Precision tests of the pseudofermion method for numerical simulations of dynamical fermions on the lattice are performed using a new criterion for the control of systematic errors, based on the Schwinger–Dyson equations.

A lattice version of the two-dimensional N fermion Gross–Neveu model, based on Wilson fermions and Symanzik's improvement scheme, is completely analyzed in the large-N expansion, up to $O(1/N)$. An unambiguous definition for the perturbative part of operators mixing with the vacuum ("condensates") is presented and discussed. Finite lattice effects are also examined.

A Monte Carlo simulation of the model is performed for different values of the coupling in the scaling region, taking into account the effects of the variation of the simulation parameters.

Comparison of analytical and numerical results shows a small but systematic difference, mainly due to an imprecise determination of the critical mass.

1. Introduction

In recent years, a number of results have been obtained in the numerical analysis of lattice field theories with fermions by use of the so-called quenched approximation in Monte Carlo simulations [1, 2]. These results strongly suggest that a more complete analysis, involving the full dynamical effect of fermion fields, would be appropriate in order to determine physical quantities, in a scheme where systematical errors are under control and statistical errors are small. The major problems that are to be faced when dealing with dynamical fermions essentially belong to the following two classes:

(i) one has to find a satisfactory algorithm to include fermion effects, fast enough to allow for the use of sufficiently big lattices but such that systematical errors are always under control;

(ii) one must be able to check the restoration of symmetries, like chirality and supersymmetry, that must be explicitly broken in order to give a correct lattice formulation of fermion fields without doubling problems.

At present the two algorithms that seem to be the best candidates for fermion simulations are the *Langevin* [3–6] and the *pseudofermion* [7–11] method. A number of tests have been performed on the first, whose advantages and drawbacks are now

more or less known [12,13]. We shall focus on the pseudofermion approach, with the purpose of giving it a comparable status.

In order to check the fermion simulation algorithm and study symmetry restoration, we decided to start from two-dimensional models. Motivations for this are both practical and theoretical. It is obvious that working in two dimensions allows for bigger lattices within reasonable limits of computer resources. Finite-volume, thermalization and boundary-condition dependence effects can be studied in greater detail, as well as long-range correlations in the number of sweeps.

From a theoretical point of view, two-dimensional models can be viewed as an important laboratory to check a number of approximation schemes applied in field theory. Most phenomena thought to be relevant in four-dimensional gauge theories have illustrations in two-dimensional models; we just mention asymptotic freedom, dynamical mass generation, and existence of $1/N$ expansions.

Chirality and supersymmetry can be defined, and even if continuous symmetries cannot be spontaneously broken because of Coleman's theorem, their realization may be highly non-trivial (Kosterlitz–Thouless phenomenon). A crucial motivation is, however, the fact that many two-dimensional asymptotically free fermionic, bosonic and mixed models, with $O(N)$ and $SU(N)$ internal symmetries, can be explicitly solved in the $N \to \infty$ limit. Moreover, semiclassical methods (DHN) allow for the determination of the mass spectra of the continuum theories, and factorizability leads to a determination of the exact S matrix for a wide class of these models. Therefore, the check of systematic and statistical errors can be made in an absolute and explicit way.

Having in mind further extensions to models with continuous symmetries, we start from the study of the N fermion Gross–Neveu model [14], a purely fermionic system with a discrete γ_5 symmetry whose dynamical breakdown leads to mass generation. This model has an exact large-N solution and is $1/N$ expandable [15,16]. The continuum Gross–Neveu model can be solved using Bethe-ansatz techniques [17]. Its bound state and soliton spectrum [18,19], as well as its factorized S matrix [20,21], are analytically known.

We mention that the Gross–Neveu model admits a chiral extension, and that the two models can be properly combined with $O(N)$ and CP^{N-1} sigma models, respectively, in order to build up $N = 1$ ($N = 2$) supersymmetric models whose properties in the continuum limit are also well known.

In sect. 2, we discuss the pseudofermion algorithm for the simulation of dynamical fermions, with special stress on the sources of systematic errors, and present a new test, based on the Schwinger–Dyson equations, allowing for a precise measurement of these errors.

In sect. 3, we review briefly the (massive) Gross–Neveu model in the continuum, and compute exactly the $1/N$ corrections to the fermion condensate.

In sect. 4, we discuss the same model on the lattice, both in the simplest version based on Wilson fermions [22,23] and in a tree-improved Symanzik formulation

[24, 25], and we exhibit the phase diagrams of the model, as a function of the (bare) mass and coupling constant.

In sect. 5, we analyze the weak-coupling phase in the large-N limit, arguing in favor of a Symanzik-improved action for all computational purposes.

In sect. 6, we discuss the finite-size effects, showing that the choice of antiperiodic boundary conditions, besides eliminating all zero-mode pathology, leads to a naïve scaling dependence of the finite-lattice effects, and this dependence can be expressed in terms of a universal function, independent of the specific features of the fermion propagator regularization.

In sect. 7, we compute the first order of the $1/N$ expansion of the model and determine numerically the set of expectation values to be reproduced by the computer simulation. We show that, in the $f \to 0$ limit, universality is satisfied and the continuum results are reproduced. To this purpose, we must define unambiguously the perturbative part of physical operators, as discussed in detail in appendix A.

Sects. 8 and 9 are devoted to the procedures and techniques of the Monte Carlo simulation.

In sect. 10 we present and discuss our numerical results. The violations of the Schwinger–Dyson equations (deviations from detailed balance) do not show the expected linear behaviour on the upgrading step squared. The pseudofermion algorithm allows for efficient determination of critical mass, but the results are not in very good agreement with the theory; this error is reflected by small but systematic deviations in other observables.

2. The algorithm for dynamical fermions

A major problem in numerical simulations of field theories is the presence of dynamical fermions. In order to avoid integration over anticommuting variables, it is necessary to integrate the fermions out explicitly, by the use of the Matthews–Salam formula

$$\int \mathrm{d}\psi\, \mathrm{d}\bar{\psi} \exp(-\bar{\psi} K \psi) = (\det K)^N, \tag{2.1}$$

where K is the Dirac operator that depends on the bosonic fields ϕ coupled to the fermions, and N is the number of (degenerate) fermion species. The resulting effective action is therefore

$$S_{\mathrm{eff}} = S_{\mathrm{b}} + S_{\mathrm{f}}, \tag{2.2}$$

where $S_{\mathrm{b}}(\phi)$ is the purely bosonic part of the original lagrangian and

$$S_{\mathrm{f}}(\phi) = -N \operatorname{Tr} \ln K(\phi). \tag{2.3}$$

The main problem arising from this formulation is the nonlocality of the fermionic determinant. In a numerical simulation this implies that the computation of the variation of S_{eff} due to the change of a single bosonic variable (i.e. the main ingredient of any algorithm) involves many other variables distributed over the lattice, and therefore it typically implies a growth in computation time proportional to V^2 instead of V (V is the lattice volume, i.e. the number of sites).

As a consequence, exact simulations of fermionic theories can be performed only on very small lattices, and in order to consider reasonably big lattices one needs some approximation scheme.

A few methods have been proposed involving computations proportional to V. Among them we mention the microcanonical method [26–29], discretized Langevin algorithms and the pseudofermion method.

We shall not discuss the microcanonical method. In order to avoid the assumption of ergodicity one has to resort to hybrid algorithms [27, 28] that are beyond the scope and limits of the present work.

Langevin and pseudofermion methods have a comparable status. In particular, the Langevin approach has a reasonably good theoretical status, including some control over the properties of the systematic errors [9]. There is only one parameter controlling these errors, the discrete step in Langevin time, and the discrete stochastic process converges to an equilibrium differing from the continuum one by terms linear in the discrete time step.

Our aim is to perform a numerical analysis of the systematic errors of the pseudofermion method within a model whose solutions can be explicitly computed, thus verifying the proposed parametrization of the errors in terms of the parameters of numerical simulation. For our purposes, let us recall the basic ideas of the pseudofermion method.

The basic ingredient consists in expanding the change in the fermionic effective action S_{f} due to the updating of the bosonic variables to the lowest order in the variation of the bosonic field itself $\delta\phi$, that is assumed to be small. In this approximation

$$\delta S_{\text{f}} \cong -N \operatorname{Tr}(K^{-1}\,\delta K) \cong -N \operatorname{Tr}\left(K^{-1}\frac{\delta K}{\delta\phi}\right)\delta\phi. \tag{2.4}$$

The updating of ϕ is performed following the Metropolis algorithm, by defining

$$\delta S_{\text{eff}} = S_{\text{b}}(\phi+\delta\phi) - S_{\text{b}}(\phi) + \delta S_{\text{f}}, \tag{2.5}$$

and using the approximation (2.4) for δS_{f}.

Consistently with this linear expansion in $\delta\phi$, we can avoid taking into account the variation of K^{-1} due to every updating of ϕ's, but compute K^{-1} only once, before updating all the bosonic fields.

The most efficient way of computing K^{-1} is by Monte Carlo inversion

$$K_{ij}^{-1}(\phi) = \langle \chi_i \chi_j^\dagger \rangle , \tag{2.6}$$

where the average is computed by introducing the quadratic action

$$S_\chi = \chi_i^\dagger K_{ij}(\phi) \chi_j \tag{2.7}$$

for the auxiliary bosonic fields χ (pseudofermions). When K is not hermitian and positive definite, the same method is applied to the inversion of $K^\dagger K$. Monte Carlo inversion has the advantage of computing only the matrix elements of K^{-1} entering $\mathrm{Tr}(K^{-1}\,\delta K)$, with computation time proportional to V, thanks to the locality of K. The sources of systematic errors are essentially two.

(i) The linear expansion of S_f and the use of K^{-1} computed at the beginning of each bosonic upgrading sweep. This implies an explicit violation of the detailed balance, that can be kept small by choosing a small step size $\delta\phi$ in the bosonic field updating. In turn, a small $\delta\phi$ slows down the dynamics of the bosonic field and requires a bigger number of sweeps in order to generate the same statistical sample of configurations;

(ii) Monte Carlo inversion of K introduces a statistical error in the matrix elements of K^{-1}, whose effect is the introduction of a noise source in the effective action

$$\delta S_f \to -N\,\mathrm{Tr}\left[(K^{-1} + \varepsilon) \frac{\delta K}{\delta \phi} \right] \delta\phi , \tag{2.8}$$

where ε is the noise matrix, that is proportional to $1/\sqrt{n_{pf}}$, where n_{pf} is the number of pseudofermionic sweeps used to compute K^{-1}. The net effect of this noise is to produce an $O(1/n_{pf})$ systematic error in the expectation value of every observable.

We will rescale the number n_{sw} of (bosonic) sweeps in order to keep constant the statistical significance of our configuration sample: $n_{sw} \propto 1/\langle(\delta\phi)^2\rangle$. In this case, according to ref. [9] systematic error (ii) should scale as $\langle(\delta\phi)^2\rangle$.

The dependence expressed in eq. (2.8) allows for a formulation of an exact theory of the deviations from the exact quantum expectation values of any observable due to the finite number of pseudofermionic sweeps. These deviations will be examined more carefully in sect. 8 for the Gross–Neveu model. The effect of Monte Carlo inversion being under control, it is crucial to investigate the effect of the step size.

To this purpose, we devised a very simple quantitative test of violation of the detailed balance.

Let us consider the total variation of the effective action,

$$\delta S_{\text{eff}} = \delta S_{\text{b}} + \delta S_{\text{f}}\,, \tag{2.9}$$

and notice that, when equilibrium is reached, the quantum field equations of the model

$$\left\langle \frac{\delta S_{\text{b}}}{\delta \phi} \right\rangle = -\left\langle \frac{\delta S_{\text{f}}}{\delta \phi} \right\rangle = N\left\langle \operatorname{Tr} K^{-1} \frac{\delta K}{\delta \phi} \right\rangle \tag{2.10}$$

are satisfied.

Both sides of eq. (2.10) are observable quantities that can be measured in the numerical simulation. Therefore, the deviation from the exact Schwinger–Dyson equation (2.10) is a precise measure of the systematic error, and for sufficiently small $\delta\phi$ this quantity should be proportional to $\langle(\delta\phi)^2\rangle$. Error propagation should then, in principle, allow one to reconstruct the effect of this error on other observable quantities.

3. The massive Gross–Neveu model

In order to fix the notation and for immediate comparison we briefly review the continuum limit of the (euclidean) two-dimensional massive Gross–Neveu model. The starting point is a theory of N self-interacting Dirac fermions with global symmetry U(N) and euclidean action

$$S = \int \mathrm{d}^2x \left[\bar{\psi}\partial\!\!\!/\psi - \tfrac{1}{2}g^2(\bar{\psi}\psi)^2 + m\bar{\psi}\psi \right]. \tag{3.1}$$

This action is stable under renormalization because of a hidden O($2N$) symmetry [18] enjoyed by the scalar interaction.

Moreover, in the limit $m \to 0$ a discrete chiral symmetry

$$(\psi, \bar{\psi}) \to (\gamma_5\psi, -\bar{\psi}\gamma_5) \tag{3.2}$$

becomes effective.

In practice, one usually prefers to eliminate the explicit four-fermion interaction by means of a Lagrange multiplier σ, such that the effective action becomes

$$S(\sigma, \psi) = \int \mathrm{d}^2x \left[\bar{\psi}\partial\!\!\!/\psi + (\sigma + m)\bar{\psi}\psi + \frac{1}{2g^2}\sigma^2 \right]. \tag{3.3}$$

One should stress that the effective action (3.3) is no longer stable under renormalization; a quartic fermion counterterm is dynamically generated by the two-loop contributions to the four-point function, corresponding to an $O(g^6)$ and $O(1/N^2)$ correction [30]. In trying to extract physical information from the effective version of the model, we must therefore keep in mind this limitation.

The $1/N$ expansion of the model is obtained by defining the operator

$$K = \partial\!\!\!/ + \sigma + m, \tag{3.4}$$

and integrating over the fermionic fields, which leads to the action

$$S_{\text{eff}}(\Sigma) = \frac{N}{2f}\int \mathrm{d}^2x(\Sigma(x) - m)^2 - N\,\mathrm{Tr}\ln K, \tag{3.5}$$

where we have defined the large-N variables

$$\Sigma = \sigma + m, \qquad f = g^2N, \qquad K(p) = ip\!\!\!/ + \Sigma. \tag{3.6}$$

The large-N solution is obtained by solving the saddle-point equation

$$\frac{1}{f}(\Sigma(x) - m) = \mathrm{tr}\,K^{-1}(x, x; \Sigma) \tag{3.7}$$

for a constant field Σ_c, playing the rôle of the effective (large-N) mass for the fermion field.

The renormalized gap equation can be expressed in the form

$$m = \frac{f}{\pi}\Sigma_c \ln\left|\frac{\Sigma_c}{\Sigma_0}\right|, \tag{3.8}$$

where

$$\Sigma_0 = \Lambda_c \exp\left(-\frac{\pi}{f}\right), \tag{3.9}$$

and is shown in fig. 1. When $m \to 0$, $\Sigma_c \to \pm\Sigma_0$, indicating a spontaneous breakdown of the discrete symmetry and a non-perturbative dynamical mass generation. The general phase diagram of this model in the (m, f) plane is shown in fig. 2.

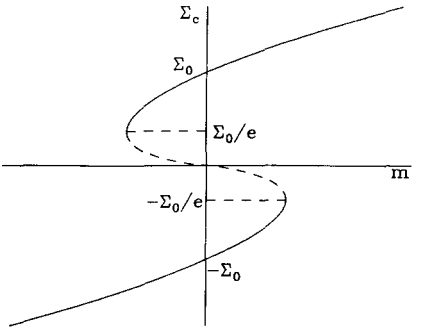

Fig. 1. The saddle-point equation of the continuum Gross-Neveu model. The dashed line is the unstable region.

In order to include the $1/N$ corrections, one has to introduce the propagator of the Σ field

$$\Delta_{\Sigma}^{-1} = \frac{\delta^2 S_{\text{eff}}(\Sigma)}{\delta\Sigma(x)\,\delta\Sigma(y)}\bigg|_{\Sigma=\Sigma_c} = N\left[\frac{1}{f} + \Pi(x,y)\right]_{\Sigma=\Sigma_c}, \tag{3.10}$$

where [14]

$$\Pi(k) = \operatorname{tr}\int \frac{\mathrm{d}^2 p}{(2\pi)^2} K^{-1}(p,\Sigma) K^{-1}(p+k,\Sigma) = \frac{1}{2\pi}\ln\left(\frac{\Sigma^2}{\Lambda_c^2}\right) + \frac{1}{2\pi}\xi\ln\left(\frac{\xi+1}{\xi-1}\right),$$

$$\xi = \sqrt{1+\frac{4\Sigma^2}{k^2}}\,. \tag{3.11}$$

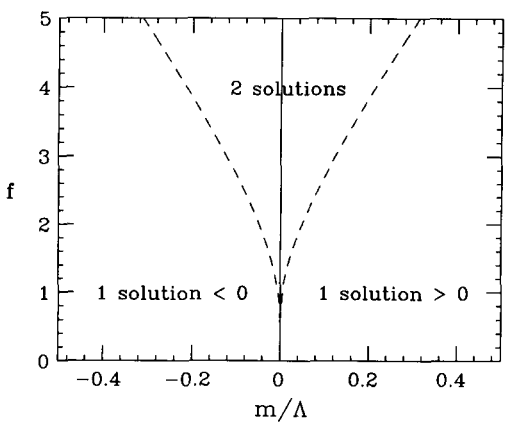

Fig. 2. Phase diagram of the continuum Gross-Neveu model. Dashed lines are the metastable phase boundaries.

The quantum effective potential, as a function of the external background field Σ, has a $1/N$ expansion

$$\Gamma(\Sigma) = N\Gamma_0(\Sigma) + \Gamma_1(\Sigma) + O(1/N), \tag{3.12}$$

where

$$\Gamma_0(\Sigma) = \frac{(\Sigma - m)^2}{2f} - \int \frac{d^2p}{(2\pi)^2} \ln(p^2 + \Sigma^2) = \frac{m^2}{2f} - m\frac{\Sigma}{f} + \frac{\Sigma^2}{4\pi}\left[\ln\left(\frac{\Sigma^2}{\Sigma_0^2}\right) - 1\right],$$

$$\Gamma_1(\Sigma) = \frac{1}{2}\int \frac{d^2p}{(2\pi)^2} \ln\left[\frac{1}{N}\Delta_\Sigma^{-1}(p)\right]. \tag{3.13}$$

The $1/N$ corrections to Σ_c can easily be expressed in terms of these functions by substituting

$$\Sigma = \Sigma_c^0 + \frac{1}{N}\Sigma_c^1 \tag{3.14}$$

into the gap equation $\partial\Gamma/\partial\Sigma = 0$, and expanding in powers of $1/N$. The result is

$$\Sigma_c^1 = -\frac{\Gamma_1'(\Sigma_c^0)}{\Gamma_0''(\Sigma_c^0)}, \tag{3.15}$$

where

$$\Gamma_1'(\Sigma) = \frac{1}{2}\int \frac{d^2p}{(2\pi)^2}\left\{\xi \ln\left(\frac{\xi+1}{\xi-1}\right)\Big/\left[\ln\left(\frac{\Sigma^2}{\Sigma_0^2}\right) + \xi \ln\left(\frac{\xi+1}{\xi-1}\right)\right]\right\}\frac{4\Sigma}{p^2 + 4\Sigma^2}, \tag{3.16}$$

$$\Gamma_0''(\Sigma) = \frac{1}{\pi} + \frac{1}{2\pi}\ln\left(\frac{\Sigma^2}{\Sigma_0^2}\right). \tag{3.17}$$

In the massless limit is is therefore possible to compute analytically Σ_c^1. We find that, when $\Sigma_c^0 = \pm\Sigma_0$

$$\Sigma_c^1 = -\frac{1}{2}\pi\int \frac{d^2p}{(2\pi)^2}\frac{\pm 4\Sigma_0}{p^2 + 4\Sigma_0^2} = \pm\Sigma_0 \ln\left|\frac{2\Sigma_0}{\Lambda_c}\right|. \tag{3.18}$$

Eq. (3.18) is found to be in agreement with the standard renormalization-group analysis of the model. It is indeed possible to write down a renormalization-group

equation for the effective potential, ignoring the above-mentioned $O(1/N^2)$ effects; in the massless limit it takes the form

$$\left[-\Lambda_c\frac{\partial}{\partial\Lambda_c}+\beta\frac{\partial}{\partial f}+\gamma\Sigma\frac{\partial}{\partial\Sigma}\right]\Gamma(\Sigma,f)=0. \tag{3.19}$$

Consistently with ref. [30], we found that the following relationships hold

$$\beta(f)=-\frac{N-1}{\pi N}f^2(1-\gamma(f))+O\left(\frac{f^4}{N^2}\right),$$

$$\gamma(f)=\frac{1}{2\pi N}f+\frac{N-1}{4\pi^2N^2}f^2+O\left(\frac{f^3}{N}\right). \tag{3.20}$$

As a consequence, we found that $\Gamma(\Sigma,f)$ is minimized by

$$\Sigma\cong\pm\bar{\Lambda}_c\exp\left\{-\frac{\pi N}{N-1}\frac{1}{f}+O\left(\frac{f}{N^2}\right)\right\}, \tag{3.21}$$

where $\bar{\Lambda}_c$ has calculable $1/N$ corrections with respect to Λ_c and no logarithmic corrections are present.

4. The Gross–Neveu model on the lattice: Generalities

A naïve transcription of the fermionic Lagrangian on a lattice leads to a species duplication [31–33]. In order to avoid this problem, we shall essentially follow Wilson's proposal [22]: degeneracies are lifted by the introduction of an irrelevant operator whose naïve continuum limit is zero.

As an unavoidable consequence, chiral invariance is explicitly broken. This is, however, a way to generate the correct chiral anomalies that otherwise would not arise in an intrinsically finite scheme such as lattice regularization. One must check that no lattice artifacts, or anomalies, that are absent in the continuum formulation, are generated in this scheme.

Another problem in two-dimensional theories arises in connection with the severe infrared divergencies that make Monte Carlo simulations very sensitive to volume effects. A better control of volume effects is obtained by the use of Symanzik's improved actions [24], reducing the effects due to the finiteness of the lattice spacing and therefore allowing for larger correlation lengths. A rather general ansatz for

lattice actions, allowing for improvement up to $O(a^2)$, is

$$
\begin{aligned}
S = a^2 \sum_x \Bigg\{ & \sum_\mu \bar{\psi}(x)\gamma_\mu \Bigg[\frac{1+4c}{2a}\big(\psi(x+a\hat{\mu}) - \psi(x-a\hat{\mu})\big) \\
& \qquad - \frac{c}{a}\big(\psi(x+2a\hat{\mu}) - \psi(x-2a\hat{\mu})\big) \Bigg] \\
& - \frac{r_1}{2a} \sum_\mu \bar{\psi}(x)\big[\psi(x+a\hat{\mu}) + \psi(x-a\hat{\mu}) - 2\psi(x)\big] \\
& + \frac{r_2}{2a} \sum_\mu \bar{\psi}(x)\big[\psi(x+2a\hat{\mu}) + \psi(x-2a\hat{\mu}) - 4\psi(x+a\hat{\mu}) \\
& \qquad - 4\psi(x-a\hat{\mu}) + 6\psi(x)\big] \\
& + m\bar{\psi}(x)\psi(x) + \sigma(x)\bar{\psi}(x)\psi(x) + \frac{1}{2g^2}\sigma^2(x) \\
& - \tfrac{1}{2}\delta_2 N \sum_\mu \sigma(x)\big[\sigma(x+a\hat{\mu}) + \sigma(x-a\hat{\mu}) - 2\sigma(x)\big] \\
& + a\delta_3 N\big(\sigma(x)+m\big)^3 + a^2\delta_4 N\big(\sigma(x)+m\big)^4 \Bigg\}. \qquad (4.1)
\end{aligned}
$$

If all coefficients $r_1, r_2, c, \delta_2, \delta_3, \delta_4$ are chosen to be equal to zero, one obtains the naïve action with species doubling. The choice $r_1 = r \neq 0$, $r_2 = c = \delta_2 = \delta_3 = \delta_4 = 0$ corresponds to the standard Wilson action.

Finally, Symanzik's improvement program is implemented by requiring the proper lattice Green functions to reproduce the corresponding continuum limit to the desired precision. The inverse fermionic propagator is

$$
\begin{aligned}
\Delta_{\mathrm{f}}^{-1} &= \sum_\mu i\gamma_\mu \bar{p}_\mu + \mathscr{M}(p) + m, \\
\bar{p}_\mu &= \frac{1}{a}\sin ap_\mu\big(1 + 2a^2 c\hat{p}_\mu^2\big), \\
\mathscr{M}(p) &= \tfrac{1}{2}ar_1\hat{p}^2 + \tfrac{1}{2}a^3 r_2 \sum_\mu \hat{p}_\mu^4, \\
\hat{p}_\mu &= \frac{2}{a}\sin \tfrac{1}{2}ap_\mu, \qquad \hat{p}^2 = \sum_\mu \hat{p}_\mu^2. \qquad (4.2)
\end{aligned}
$$

Expanding in powers of a, one obtains

$$\Delta_{\mathrm{f}}^{-1}(p) \to \sum_{\mu} i\gamma_\mu p_\mu \left[1 + \left(2c - \tfrac{1}{6}\right) a^2 p_\mu^2\right] + \tfrac{1}{2} r_1 a p^2 + \tfrac{1}{2}\left(r_2 - \tfrac{1}{12} r_1\right) a^3 \sum_{\mu} p_\mu^4 + m\,. \tag{4.3}$$

Therefore Symanzik's tree improved action is obtained through the choices

$$c = \tfrac{1}{12}\,, \qquad r_1 = 0\,. \tag{4.4}$$

One-loop perturbative computation of two, three and four-point Green functions for the field σ allows for the determination of δ_2, δ_3 and δ_4 and the construction of the one-loop improved Symanzik action.

The form of one-loop improvement assumed in eq. (4.1) can be shown to imply that no deviations from asymptotic scaling are present for physical quantities, up to $\mathrm{O}(\exp(-4\pi/f))$, thus solving the apparent paradox of ref. [25].

For our present purposes, we only need to focus on the behavior of Wilson and Symanzik's tree-improved actions, with special emphasis on their exactly solvable large-N limit.

We introduce the large-N effective potential in the form

$$\Gamma_0(\Sigma) = \frac{1}{2f}(\Sigma - m)^2 + F_0(\Sigma) + \delta_3 \Sigma^3 + \delta_4 \Sigma^4\,, \tag{4.5}$$

where

$$F_0(\Sigma) = -\operatorname{tr} \int \frac{\mathrm{d}^2 p}{(2\pi)^2} \ln\left[i\not{p} + \mathscr{M}(p) + \Sigma\right], \tag{4.6}$$

and study the different phases of the models in the (m, f) plane by considering the saddle-point equation (when $\delta_3 = \delta_4 = 0$)

$$\frac{\Sigma - m}{f} + F_0'(\Sigma) = 0\,. \tag{4.7}$$

In general, eq. (4.7) has more than one solution. The absolute minimum of $\Gamma_0(\Sigma)$ is the true vacuum of the model; other solutions that are local minima correspond to metastable states. Varying m and f leads to level crossing: first-order transition lines separating different stable phases correspond to values of the parameters such that two degenerate vacua are present.

The appearance of a new solution is related to the simultaneous solution of eq. (4.7) and its first derivative

$$\frac{1}{f} + F_0''(\Sigma) = 0. \tag{4.8}$$

We can therefore find immediately the end lines of the different metastable phases in the form of a parametric equation in Σ

$$\begin{cases} m = \Sigma - \dfrac{F_0'(\Sigma)}{F_0''(\Sigma)}, \\ f = -\dfrac{1}{F_0''(\Sigma)}. \end{cases} \tag{4.9}$$

The Wilson-action phase diagram is presented in fig. 3 for the choice $r_1 = 1$. The symmetry of the effective potential under the exchange

$$(m + 2r_1) \to -(m + 2r_1), \qquad \sigma \to -\sigma \tag{4.10}$$

manifests itself in the structure of the phase diagram. As discussed in ref. [23], this symmetry implies the existence of three different weak-coupling phases: a Kogut–Susskind phase with fermion doubling around $m = -2r_1$, $f = 0$, and two equivalent and separate chiral phases around $m = 0$, $f = 0$ and $m = -4r_1$, $f = 0$.

The Symanzik tree-level improved action does not possess the above-mentioned symmetry. The appearance of new vacua occurs now for nonzero values of f, as shown in the phase diagram of fig. 4, for $r_2 = \frac{1}{3}$.

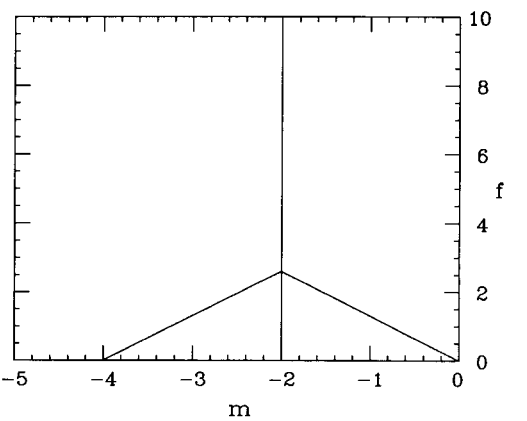

Fig. 3. Phase diagram for Wilson action, with $r_1 = 1$.

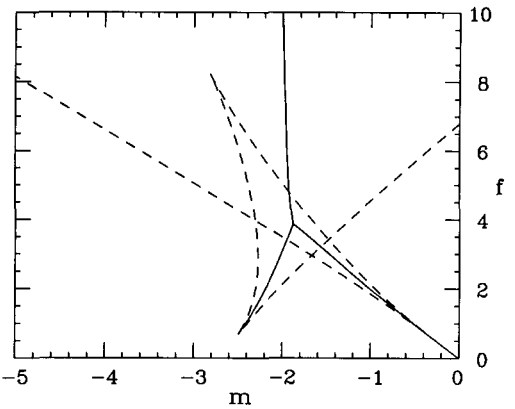

Fig. 4. Phase diagram for Symanzik action, with $r_2 = \frac{1}{3}$. Solid lines are the phase-transition lines; dashed lines are the metastable phase boundaries.

For very large f, the two models become comparable, the strong-coupling chiral line being $m = -2r_1$ for Wilson action and tending asymptotically to $m = -6r_2$ for Symanzik tree action. This fact allows for a direct comparison between values of r_1 and r_2 related by

$$r_2 = \tfrac{1}{3} r_1 . \tag{4.11}$$

This relationship qualitatively survives when we compare the weak-coupling regimes of the two models and is one of the justifications for the choice $r_2 = \frac{1}{3}$ in our actual computations.

5. The weak-coupling phase

In order to make more quantitative theoretical statements about the physics of the lattice Gross-Neveu model in the different formulations that have been presented, we need to consider the weak-coupling expansion of the effective potential near the chiral limit. In this section we shall still focus on the large-N limit of the model. Most statements which are valid in this limit will, however, turn rather immediately into more general properties of the model at arbitrary (not too small) N.

Since $\Sigma_0 \sim \exp(-\pi/f)$, the weak-coupling expansion will turn into a small-Σ expansion for the function $F_0(\Sigma)$ appearing in the large-N effective potential. In general, the following expression will hold

$$F_0(\Sigma) \simeq a_0 + a_1\Sigma + \sum_{n=2}^{\infty} (a_n + b_n \ln|\Sigma|)\Sigma^n , \tag{5.1}$$

where the coefficients a_n, b_n will depend on the parameters r_1, r_2 and c.

In the naïve chiral limit $r_1 = r_2 = 0$, the coefficients of the odd terms a_{2n+1}, b_{2n+1} will vanish.

In general, the nth coefficients are associated, by naïve power counting, with the power a^{n-2} of the lattice spacing a. In particular, $a_0 \sim a^{-2}$ is an irrelevant overall constant in the vacuum energy, and $a_1 \sim a^{-1}$ is, in the large-N limit, the perturbative mass renormalization of the fermion. All terms such that $n \geq 3$ are nonperturbatively depressed like $\exp(-n\pi/f)$ in the weak-coupling regime and correspond to the contribution of irrelevant operators, vanishing in the naïve continuum limit $a \to 0$.

One more piece of information comes from an analysis of the infrared behavior of the momentum integral in eq. (4.6), showing that

$$b_2 = \frac{1}{2\pi}, \qquad b_3 = \frac{r_1}{2\pi}, \tag{5.2}$$

while b_4 vanishes for arbitrary r_2 when $r_1 = 0$ and $c = \frac{1}{12}$. Therefore $b_3 = b_4 = 0$ for Symanzik's tree improved action, as required by its definition.

Finally, Symanzik's one-loop improvement corresponds to the choice $\delta_3 = -a_3$, $\delta_4 = -a_4$ (δ_2 is computed in appendix B). The coefficients a_0, a_1 and a_3 have simple representations in terms of momentum integrals

$$a_0 = -\int \frac{d^2p}{(2\pi)^2} \ln\left(\bar{p}^2 + \mathcal{M}^2\right),$$

$$a_1 = -\int \frac{d^2p}{(2\pi)^2} \frac{2\mathcal{M}}{\bar{p}^2 + \mathcal{M}^2},$$

$$a_3 = \int \frac{d^2p}{(2\pi)^2} \frac{2\mathcal{M}\left(\bar{p}^2 - \frac{1}{3}\mathcal{M}^2\right)}{\left(\bar{p}^2 + \mathcal{M}^2\right)^3} \qquad \text{(only if } r_1 = 0\text{)}. \tag{5.3}$$

In order to define a_2, a subtraction of the logarithmic singularity must be performed, thus obtaining

$$a_2 = -\frac{1}{4\pi}(1 + 5\ln 2) - \int \frac{d^2p}{(2\pi)^2} \left[\frac{\bar{p}^2 - \mathcal{M}^2}{\left(\bar{p}^2 + \mathcal{M}^2\right)^2} - \frac{1}{\hat{p}^2} \right]. \tag{5.4}$$

We can now define (unconventionally) the Λ parameter of the model in the large-N limit

$$\lim_{f \to 0} a\Lambda_c \equiv \Lambda = \exp\left[-2\pi \left(a_2 + \frac{1}{4\pi} \right) \right]. \tag{5.5}$$

The expansion of the effective potential including the first irrelevant operators is therefore (up to a constant)

$$\Gamma_0(\Sigma) \cong \frac{1}{2f}\Sigma^2 + \left(a_1 - \frac{m}{f}\right)\Sigma + \frac{1}{4\pi}\left(\ln\left(\frac{\Sigma^2}{\Lambda^2}\right) - 1\right)\Sigma^2 + \left(a_3 + \frac{r_1}{2\pi}\ln|\Sigma|\right)\Sigma^3. \quad (5.6)$$

The numerical values of the lowest order coefficients, for $r_2 = \frac{1}{3}$, are

$$a_1 = -0.512165, \qquad a_2 = -0.136823,$$

$$a_3 = \ \ 0.061009, \qquad a_4 = -0.027964,$$

$$a_5 = -0.011944, \qquad b_5 = \ \ 1/(8\pi), \quad (5.7)$$

and therefore $\Lambda = 1.432877$.

We can now search for solutions of the saddle-point equations corresponding to a pair of degenerate minima of the effective action, i.e. satisfying the set of equations [23]

$$\Gamma_0(\Sigma_+) = \Gamma_0(\Sigma_-),$$

$$\frac{\delta\Gamma_0}{\delta\Sigma}(\Sigma_+) = \frac{\delta\Gamma_0}{\delta\Sigma}(\Sigma_-) = 0. \quad (5.8)$$

When f is sufficiently small, we find (for $r_1 = 0$)

$$m^0 \cong fa_1 + fa_3\Sigma_0^2,$$

$$\Sigma_\pm^0 \cong \pm\Sigma_0 - 2\pi a_3\Sigma_0^2, \quad (5.9)$$

where $\Sigma_0 = \Lambda\exp(-\pi/f)$.

One-loop improvement would correspond to vanishing of the $O(\Sigma_0^3)$ corrections in the physical quantity $\frac{1}{2}(\Sigma_+^0 - \Sigma_-^0)$.

An example of the behavior of the effective potential $\Gamma_0(\Sigma)$ for a few values of m around the critical mass is shown in fig. 5. In table 1 the values of Σ_+^0, Σ_-^0 and m^0, obtained by numerical solutions of the exact eqs. (5.8), are presented. These values are compared with the results of eq. (5.9) in fig. 6 (the values of m^0 given by eq. (5.9) are indistinguishable from those of table 1.)

Symanzik's improvement can be quantified by noticing that the width of the scaling region is consistently measured by the biggest values of the renormalization-group-invariant quantity Σ that can be reached without leaving the weak-coupling domain.

The crossover region between weak and strong coupling can be approximately measured, for comparable values of r_1 and r_2 ($r_1 = 3r_2 = r$), by equating the weak-

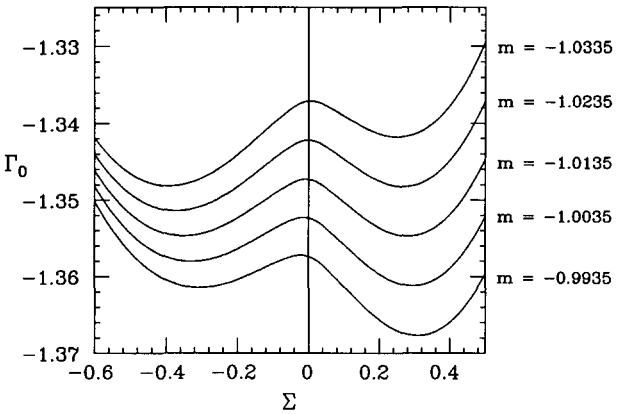

Fig. 5. The effective potential $\Gamma_0(\Sigma)$ for Symanzik action, for $r_2 = \frac{1}{3}$, $f = 2$ and values of m around $m_c = -1.0135$.

TABLE 1
Critical mass and condensate, to lowest order in $1/N$
(exact solutions of eq. (5.8))

f	Σ_0	Σ_+^0	$-\Sigma_-^0$	$-m^0$
2.5	0.40781	0.38812	0.52139	1.254888
2.4	0.38701	0.36755	0.48637	1.207211
2.3	0.36560	0.34663	0.45170	1.159239
2.2	0.34359	0.32537	0.41740	1.110976
2.1	0.32100	0.30377	0.38350	1.062426
2.0	0.29787	0.28183	0.35005	1.013592
1.9	0.27423	0.25959	0.31710	0.964480
1.8	0.25016	0.23706	0.28472	0.915197
1.7	0.22575	0.21432	0.25300	0.865453
1.6	0.20113	0.19142	0.22206	0.815559
1.5	0.17645	0.16848	0.19204	0.765428
1.4	0.15193	0.14564	0.16311	0.715078
1.3	0.12785	0.12312	0.13550	0.664529
1.2	0.10453	0.10120	0.10950	0.613804
1.1	0.08239	0.08021	0.08537	0.562928
1.0	0.06192	0.06063	0.06355	0.511932
0.9	0.04368	0.04301	0.04446	0.460844
0.8	0.02823	0.02794	0.02855	0.409693
0.7	0.01611	0.01601	0.01621	0.358504
0.6	0.007625	0.007603	0.007648	0.307297
0.5	0.002676	0.002673	0.002679	0.256082

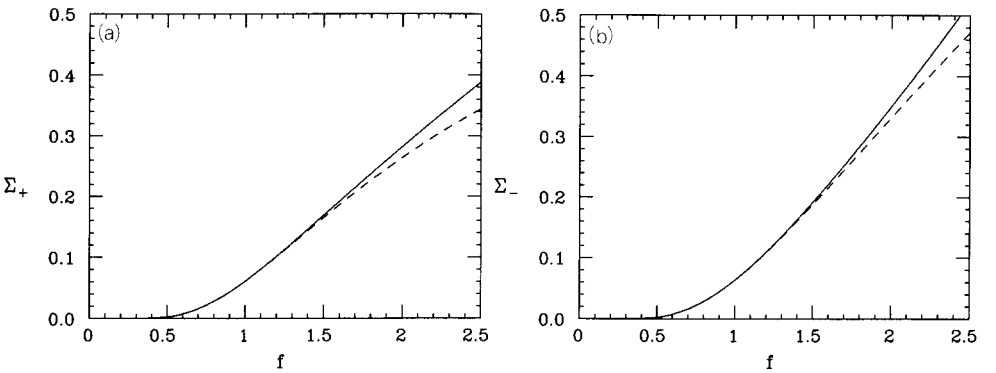

Fig. 6. Exact values of (a) Σ_+^0 and (b) Σ_-^0 (solid line), compared to expansion (5.9) (dashed line).

and strong-coupling expressions for the perturbative mass

$$f_c a_1 \approx -2r. \tag{5.10}$$

We can therefore define the quantity

$$\Sigma_c(r) = \Lambda(r)\exp\left\{-\frac{\pi}{f_c(r)}\right\} = \exp\left\{-\frac{1}{2} + \pi\left(\frac{a_1}{2r} - 2a_2\right)\right\}, \tag{5.11}$$

measuring the approximate value of the vacuum condensate in the crossover region for a given value of r. In fig. 7 the dependence of Σ_c from r for Wilson and Symanzik tree level action is presented.

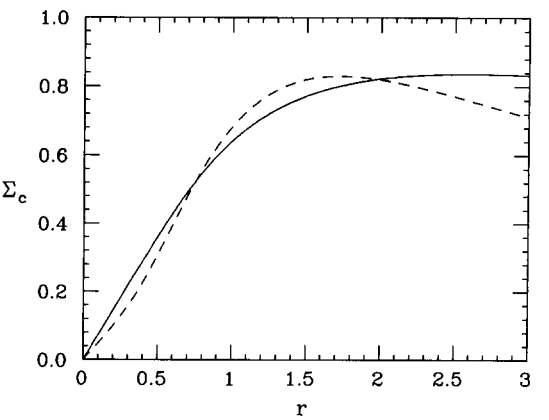

Fig. 7. Σ_c as a function of r for Wilson action (dashed line) and Symanzik action (solid line). Σ_c^{Wil} is multiplied by 4.

It is worth noticing that, consistently with our statement about the relationship between r_1 and r_2, in a wide region $0.1 \leqslant r \leqslant 2$, including our reference value $r = 1$, the ratio $\Sigma_c^{\mathrm{Sym}}/\Sigma_c^{\mathrm{Wil}}$ is approximately constant and equal to 4. In particular, for $r = 1$

$$\Lambda_{\mathrm{Wil}}/\Lambda_{\mathrm{Sym}} \cong 2.5\,, \tag{5.12}$$

implying the finite renormalization

$$\frac{1}{f_{\mathrm{Wil}}} - \frac{1}{f_{\mathrm{Sym}}} \cong -0.29\,. \tag{5.13}$$

Moreover

$$\frac{1}{f_c^{\mathrm{Wil}}} - \frac{1}{f_c^{\mathrm{Sym}}} = -\tfrac{1}{2}\left(a_1^{\mathrm{Wil}} - a_1^{\mathrm{Sym}}\right) \cong 0.14\,, \tag{5.14}$$

implying altogether

$$\Sigma_c^{\mathrm{Sym}}/\Sigma_c^{\mathrm{Wil}} \cong 3.88\,. \tag{5.15}$$

In order to fully understand the practical implications of this improvement, we must, however, discuss the finite-lattice effects, which we shall do in sect. 6.

6. Finite-lattice effects

In the absence of a general theory of finite-lattice effects, we decided to resort to a detailed numerical analysis of these effects in the Gross–Neveu model by evaluating on a finite lattice the function $F_0(\Sigma)$ and its derivatives, varying all the possible relevant parameters.

We defined

$$F_0(\Sigma, L) = -\sum_p \frac{1}{L^2} \ln\left\{ \bar{p}^2 + \left(\mathscr{M}(p) + \Sigma\right)^2 \right\}, \tag{6.1}$$

where the sum runs over all the Fourier modes of a lattice of size $L \times L$, with antiperiodic boundary conditions

$$p_\mu = \frac{2\pi}{L}\left(n_\mu - \tfrac{1}{2}\right), \qquad n_\mu \text{ integer}\,. \tag{6.2}$$

The choice of antiperiodic boundary conditions was motivated by the need of eliminating all dependence from the zero modes that are integrable in the contin-

uum limit but appear as spurious singularities at $\Sigma = 0$ in the lattice formulation with periodic boundary conditions.

We studied the quantities

$$\Delta F_0(\Sigma, L) = F_0(\Sigma, L) - F_0(\Sigma, \infty),$$

$$\Delta F_0'(\Sigma, L) = F_0'(\Sigma, L) - F_0'(\Sigma, \infty),$$

$$\Delta F_0''(\Sigma, L) = F_0''(\Sigma, L) - F_0''(\Sigma, \infty), \tag{6.3}$$

for $L = 5, 10, 20, 40, 60$, $r_2 = 0.1$–2, $r_1 = 0, \frac{1}{3}, 1$, and $-10/L \leqslant \Sigma \leqslant 10/L$. Our conclusions are the following:

(i) the function $\Delta F_0(\Sigma, L)$ does not show any significant dependence on r_1, r_2 in the whole region of parameters we have considered and for all $L \geqslant 20$ at least. This statement is true up to one part in 10^3 for $L = 40$ and especially well verified when r_2 is varied at $r_1 = 0$. As a consequence, the finite-lattice dependence is a universal function that can be studied directly on the integral of the scalar propagator

$$F_0^{\text{scalar}}(\Sigma, L) = -\sum_p \frac{1}{L^2} \ln(\hat{p}^2 + \Sigma^2); \tag{6.4}$$

(ii) $\Delta F_0(\Sigma, L)$ shows naïve scaling dependence on the variable $S = \Sigma L$ for all $L \geqslant 20$, i.e.

$$\Delta F_0(\Sigma, L) = \frac{1}{L^2} f_0(S),$$

$$\Delta F_0'(\Sigma, L) = \frac{1}{L} f_0'(S),$$

$$\Delta F_0''(\Sigma, L) = f_0''(S). \tag{6.5}$$

The behavior of $f_0(S)$ is shown in fig. 8. Its main features are:

(a) an exponential decay $\sim \exp(-|S|)$ of the function for large S, with logarithmic slope essentially equal to 1;

(b) $S \to -S$ symmetry;

(c) a small-S expansion governed by the ultraviolet renormalization group of the model, implying

$$f_0(S) \approx \text{const.} - \frac{S^2}{4\pi}\left(\ln\left(\frac{S^2}{S_c^2}\right) - 1\right),$$

$$f_0''(S) \approx -\frac{1}{\pi}\left(\ln\left|\frac{S}{S_c}\right| + 1\right). \tag{6.6}$$

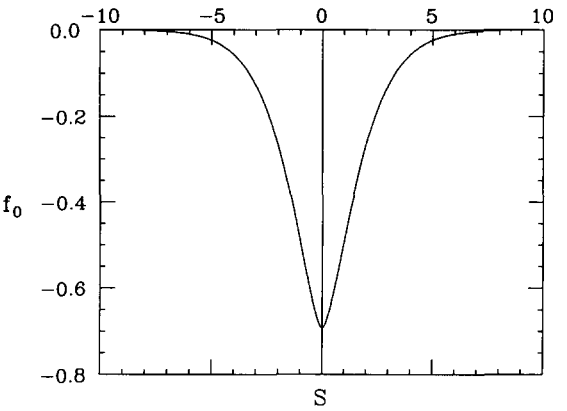

Fig. 8. $f_0(S) = L^2 \Delta F_0(\Sigma, L)$ for a 40×40 lattice.

S_c is a universal constant that can be determined from the equation

$$\ln S_c = \frac{5}{2} \ln 2 + \lim_{L \to \infty} \left(\ln L - \frac{2\pi}{L^2} \sum_p \frac{1}{\hat{p}^2} \right), \tag{6.7}$$

giving $S_c \cong 2.082$ (already verified for $L = 40$).

The variable S measures the physical dimensions of the lattice in units of the fermion correlation length, and the naïve scaling dependence shows that the finite-lattice renormalization group is the same as the ultraviolet renormalization group: $L \sim \exp(\pi/f)$. Keeping S fixed is the physically meaningful way of extracting continuum information out of the model.

As an immediate consequence, we reinterpret our equations as a condition on the lattice volume: $S \gg S_c$ implies $L \gg S_c/\Sigma$ and therefore the minimum acceptable lattice size L_c must obey $L_c \gg S_c/\Sigma_c$, implying

$$\frac{L_c^{\text{Wil}}}{L_c^{\text{Sym}}} \simeq 4. \tag{6.8}$$

The volume factor in favor of Symanzik action is ≈ 15 for $r = 1$.

7. The $1/N$ expansion

For theoretical and numerical purposes, it is extremely important to understand the rôle of the $1/N$ corrections in the lattice version of the model.

As we already mentioned in discussing the continuum version, as long as we ignore $O(1/N^2)$ effects we can apply the effective potential formalism and study the behavior of the operator Σ neglecting its compositeness.

While the renormalization-group analysis can be repeated without modifications, and the results concerning physically scaling quantities are simply a reproduction of the continuum results, the bare quantities resulting from the actual computation are necessarily affected by perturbative tails that must be theoretically understood and subtracted in order to obtain the continuum limit.

The essential ingredient of the $1/N$ expansion is the Σ field propagator, defined in eq. (3.10). The lattice representation of the self-energy part is

$$\Pi(k,\Sigma) = \int \frac{d^2p}{(2\pi)^2} \frac{2\left[(\mathscr{M}(l_1)+\Sigma)(\mathscr{M}(l_2)+\Sigma) - \bar{l}_1\cdot\bar{l}_2\right]}{\left[\bar{l}_1^2 + (\mathscr{M}(l_1)+\Sigma)^2\right]\left[\bar{l}_2^2 + (\mathscr{M}(l_2)+\Sigma)^2\right]}, \tag{7.1}$$

where $l_1 = p$ and $l_2 = p + k$.

$\Pi(k,\Sigma)$ admits a small-Σ expansion

$$\Pi(k,\Sigma) = \Pi_0(k) + \sum_{n=1}^{\infty}\left[A_n(k) + B_n(k)\ln\left(\frac{|\Sigma|}{\Lambda}\right)\right]\Sigma^n. \tag{7.2}$$

The expansion coefficients can show significant deviations from the corresponding continuum expressions. The computation of $\Pi_0(k)$ is discussed in appendix A. Its behavior is shown in fig. 9. We just mention that, in Symanzik's tree improved model

$$\Pi_0(k) \simeq \frac{1}{2\pi}\ln\left(\frac{k^2}{\Lambda^2}\right) + \Delta_2 k^2 + O(k^4), \tag{7.3}$$

where Δ_2 is related to the one-loop improvement parameter by $\delta_2 = -\Delta_2$. The next

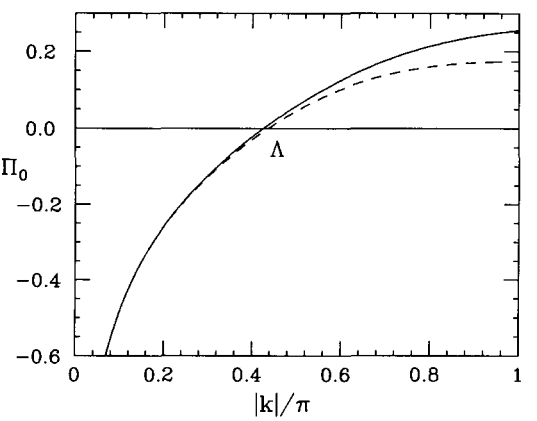

Fig. 9. $\Pi_0(k)$ computed for $k_y = k_x$ (solid line) and for $k_y = 0$ (dashed line), showing rotation invariance for $|k|/\Lambda < 1$.

terms of the expansion are

$$A_1(k) \simeq 6a_3 + \mathrm{O}(k^2),$$

$$B_1(k) = -\frac{1}{\pi}\frac{2\mathscr{M}(k)}{\bar{k}^2 + \mathscr{M}^2(k)} \simeq \mathrm{O}(k^2),$$

$$A_2(k) \simeq \frac{1}{\pi k^2}\left[\ln\left(\frac{k^2}{\Lambda^2}\right) + 1\right] + 12a_4 + \mathrm{O}(k^2),$$

$$B_2(k) = -\frac{1}{\pi}\left[2\frac{\bar{k}^2 - \mathscr{M}^2(k)}{\left(\bar{k}^2 + \mathscr{M}^2(k)\right)^2} + \sum_\mu \frac{\partial}{\partial k_\mu}\frac{\bar{k}_\mu}{\bar{k}^2 + \mathscr{M}^2(k)}\right] \simeq -\frac{2}{\pi k^2} + \mathrm{O}(k^2). \tag{7.4}$$

We report for comparison the corresponding expressions for the Wilson model [23]

$$\Pi_0(k) \simeq \frac{1}{2\pi}\ln\frac{k^2}{\Lambda_{\mathrm{W}}^2} + \mathrm{O}(|k|),$$

$$A_1(k) \simeq \frac{r}{2\pi}\ln k^2 + \text{const.} + \mathrm{O}(|k|),$$

$$B_1(k) \simeq -\frac{r}{\pi} + \mathrm{O}(|k|),$$

$$A_2(k) \propto \frac{1}{k^2}\ln k^2,$$

$$B_2(k) \propto \frac{1}{k^2}. \tag{7.5}$$

One sees that the effect of the tree-level improvement is the disappearance of all spurious logarithmic dependences on k and Σ up to $\mathrm{O}(a^2)$.

We can now study the behavior of the $1/N$ contribution to the effective potential

$$\Gamma_1(f, \Sigma) = \frac{1}{2}\int \frac{\mathrm{d}^2k}{(2\pi)^2}\ln\left(\frac{1}{f} + \Pi(k, \Sigma)\right). \tag{7.6}$$

The perturbative tail of Γ_1, defined as

$$\Gamma_1(f,0) = \frac{1}{2}\int \frac{\mathrm{d}^2k}{(2\pi)^2} \ln\left(\frac{1}{f} + \Pi_0(k)\right), \tag{7.7}$$

is an irrelevant numerical constant renormalizing the vacuum energy. There is, however, a good reason to study its dependence on f. Let us indeed consider the observable quantity

$$\left\langle \Sigma^2(x)\right\rangle - \left\langle \Sigma(x)\right\rangle^2 \equiv \left\langle \Sigma^2(x)\right\rangle_{\mathrm{c}} = \frac{1}{N} C_1\left(f, \Sigma^0_{\pm}(f)\right) + \mathrm{O}\left(\frac{1}{N^2}\right), \tag{7.8}$$

where

$$C_1(f,\Sigma) = \int \frac{\mathrm{d}^2k}{(2\pi)^2} \frac{1}{1/f + \Pi(k,\Sigma)} = -2f^2 \frac{\partial}{\partial f}\Gamma_1(f,\Sigma). \tag{7.9}$$

The perturbative tail of this quantity is related to that of Γ_1 through the relationship

$$C_1(f,0) = \int \frac{\mathrm{d}^2k}{(2\pi)^2} \frac{1}{1/f + \Pi_0(k)} = -2f^2 \frac{\partial}{\partial f}\Gamma_1(f,0). \tag{7.10}$$

$\Gamma_1(f,0)$ is a non-Borel summable asymptotic series in f

$$\Gamma_1(f,0) \sim -\tfrac{1}{2}\ln f + \sum_{n=1}^{\infty} \frac{(-1)^{n+1}}{2n} c_n f^n,$$

$$c_n = \int \frac{\mathrm{d}^2k}{(2\pi)^2} \left[\Pi_0(k)\right]^n \underset{n\to\infty}{\longrightarrow} (-1)^n n! \left(\frac{1}{2\pi}\right)^n \frac{\Lambda^2}{4\pi}. \tag{7.11}$$

Choosing $r_2 = \frac{1}{3}$, we obtain

$$c_1 \equiv \tfrac{1}{2}a_1^2 = 0.131156,$$

$$c_2 = 0.040352, \qquad c_3 = 0.003228. \tag{7.12}$$

Numerical evaluation and series resummation for $\Gamma_1(f,0)$ and $C_1(f,0)$ are discussed in appendix A.

Going back to the function $\Gamma_1(f,\Sigma)$, we notice that the argument of the logarithm in the integral is not always a positive-definite function. In the weak-cou-

pling limit the positivity condition for all k turns into the request that

$$\frac{1}{f}+\frac{1}{\pi}+\frac{1}{\pi}\ln\frac{|\Sigma|}{\Lambda}\geqslant 0,$$

i.e.

$$|\Sigma|\geqslant\frac{\Sigma_0}{\mathrm{e}}. \tag{7.13}$$

Therefore in the small-Σ region $\Gamma_1(f,\Sigma)$ develops a nonzero imaginary part, and in the limit $\Sigma\to 0$

$$\operatorname{Im}\Gamma_1(f,0)=\frac{\pi}{2}\int^{\tilde{k}}\frac{\mathrm{d}^2k}{(2\pi)^2}, \tag{7.14}$$

where $\tilde{k}$ is defined by the relationship $1/f+\Pi_0(\tilde{k})=0$. For small f we have $\tilde{k}\cong\Sigma_0(f)$ and therefore

$$\operatorname{Im}\Gamma_1(f,0)\cong\tfrac{1}{8}\Sigma_0^2, \tag{7.15}$$

a relationship that we have numerically verified. The imaginary part of $\Gamma_1(f,\Sigma)$ is a signal of the instability of the effective potential in the region of values of Σ that are physically not attainable [15]. Indeed, by comparing with eq. (3.8) and fig. 1, we recognize that the value $|\Sigma|=\Sigma_0/\mathrm{e}$ is exactly at the endpoint of the curve $\Sigma(m)$.

Aside from the perturbative tail, lattice regularization, due to the explicit breakdown of γ_5 invariance, generates terms that are odd functions of Σ in the effective potential. In particular, a linear term arises in Γ_1, inducing a $1/N$ renormalization of the mass parameter and a nonmultiplicative redefinition of the nonperturbative part of the field Σ. Including only relevant operators, we can therefore parametrize the $1/N$ correction to the effective potential in the small-coupling region by

$$\Gamma_1(f,\Sigma)\approx\Gamma_1(f,0)+\left[\bar{a}_1(f)+\bar{b}_1(f)\ln\frac{|\Sigma|}{\Lambda}\right]\Sigma+\tfrac{1}{2}\Sigma^2G_1(f,t), \tag{7.16}$$

where $t=\ln(|\Sigma|/\Lambda)$.

Going back to the definition of Γ_1, it is easy to obtain the relationships

$$\bar{a}_1(f)=\frac{1}{2}\int\frac{\mathrm{d}^2k}{(2\pi)^2}\frac{A_1(k)}{1/f+\Pi_0(k)},$$

$$\bar{b}_1(f)=\frac{1}{2}\int\frac{\mathrm{d}^2k}{(2\pi)^2}\frac{B_1(k)}{1/f+\Pi_0(k)}, \tag{7.17}$$

and the following exact equations hold

$$\int \frac{d^2k}{(2\pi)^2} A_1(k) = 0, \qquad \int \frac{d^2k}{(2\pi)^2} B_1(k) = \frac{a_1}{\pi}, \tag{7.18}$$

implying

$$\bar{a}_1(f) = O(f^2),$$

$$\bar{b}_1(f) = f\frac{a_1}{2\pi} + O(f^2). \tag{7.19}$$

$\bar{a}_1(f)$ and $\bar{b}_1(f)$ are non-Borel summable series. The behavior of $\bar{b}_1(f)$ will be shown in fig. 12 (see below).

These results are consistent with the explicit computation of the two-loop contribution to the effective potential, which can be performed analytically, and coincides with the first coefficient of the expansion of Γ_1 in powers of f

$$\tfrac{1}{2}f\int \frac{d^2k}{(2\pi)^2}\Pi(k,\Sigma) = \tfrac{1}{2}f\int \frac{d^2k}{(2\pi)^2}\,\mathrm{tr}\int \frac{d^2p}{(2\pi)^2}K^{-1}(p,\Sigma)K^{-1}(p+k,\Sigma)$$

$$= \tfrac{1}{2}f\,\mathrm{tr}\left[\int \frac{d^2k}{(2\pi)^2}K^{-1}(k,\Sigma)\right]^2 = \tfrac{1}{4}f\left[F_0'(\Sigma)\right]^2. \tag{7.20}$$

By substituting eq. (7.16) into (7.9), we obtain

$$C_1(f,\Sigma) \approx C_1(f,0) + 2\left[\dot{\bar{a}}_1(f) + \dot{\bar{b}}_1(f)\ln\frac{|\Sigma|}{\Lambda}\right]\Sigma + \Sigma^2\dot{G}_1(f,t), \tag{7.21}$$

where the dot stands for derivative respect to $1/f$.

Eq. (7.21) reflects a very general phenomenon occurring in the lattice formulation of quantum field theories: the mixing between quantum operators with the same conserved quantum numbers. In our case, the explicit breaking of the chiral γ_5 symmetry allows for perturbative mixing between the operator $\Sigma_c^2(x)$ defined by eq. (7.8) and the operator $\Sigma(x)$.

In order to decouple the two operators, we shall therefore parametrize lattice expectation values in the scaling region by

$$N\langle\Sigma^2(x)\rangle_c(f) \approx C_1(f,0) + \alpha_1(f)\langle\Sigma(x)\rangle(f) + \alpha_2(f)\left[\langle\Sigma(x)\rangle(f)\right]^2. \tag{7.22}$$

There are two different values of $\langle\Sigma^2(x)\rangle_c$ for each value of f, given by eq. (7.8) and corresponding to the large-N solutions Σ_+^0 and Σ_-^0 of table 1. These values are

TABLE 2
The $1/N$ (leading) contribution to $N\langle\Sigma^2(x)\rangle_c$, $C^1_\pm \equiv C_1(f, \Sigma^0_\pm(f))$, and its perturbative part $C^1_0 \equiv C_1(f,0)$

f	C^1_+	C^1_-	C^1_0
2.5	1.65294	2.41375	2.02306
2.4	1.61267	2.30992	1.96427
2.3	1.57150	2.20700	1.90318
2.2	1.52935	2.10491	1.83977
2.1	1.48610	2.00360	1.77399
2.0	1.44161	1.90301	1.70584
1.9	1.39572	1.80309	1.63533
1.8	1.34824	1.70382	1.56248
1.7	1.29895	1.60515	1.48738
1.6	1.24760	1.50707	1.41012
1.5	1.19391	1.40957	1.33085
1.4	1.13755	1.31266	1.24974
1.3	1.07818	1.21636	1.16702
1.2	1.01545	1.12071	1.08292
1.1	0.94908	1.02577	0.99773
1.0	0.87880	0.93161	0.91168
0.9	0.80454	0.83831	0.82499
0.8	0.72635	0.74592	0.73778
0.7	0.64452	0.65438	0.65004

presented in table 2 together with the perturbative tail $C_1(f,0)$. We can therefore determine the (approximate) values of $\alpha_1(f)$ and $\alpha_2(f)$ for each finite value of f by solving a simple linear system and studying the behavior of these functions when $f \to 0$.

The perturbative value of $\alpha_1(f)$ can be extracted from eq. (7.21) by observing that, when $f \to 0$,

$$\dot{\bar{b}}_1(f) \to -f^2 \frac{a_1}{2\pi} \tag{7.23}$$

and therefore, as shown in fig. 10,

$$\alpha_1(f) \underset{f\to 0}{\longrightarrow} f a_1 \cong m^0 . \tag{7.24}$$

The behavior of $\alpha_2(f)$ is shown in fig. 11; it is related to the wave-function renormalization of $\Sigma(x)$. Its universal term can be computed in the continuum model, leading to

$$\alpha_2(f) \underset{f\to 0}{\longrightarrow} \ln f , \tag{7.25}$$

in agreement with our numerical results.

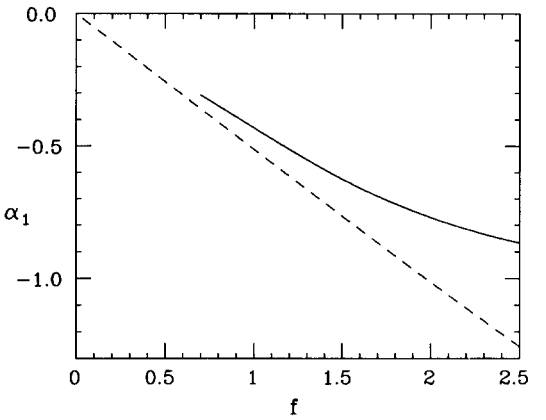

Fig. 10. The mixing coefficient $\alpha_1(f)$ (solid line), compared with m_0 (dashed line).

In order to compute the $1/N$ corrections to the vacuum expectation value of Σ, we can now substitute our results into eqs. (5.8) and solve perturbatively in $1/N$ by the ansatz

$$\Gamma = \Gamma_0 + \frac{1}{N}\Gamma_1, \qquad m = m^0 + \frac{1}{N}m^1, \qquad \Sigma_\pm = \Sigma^0_\pm + \frac{1}{N}\Sigma^1_\pm . \tag{7.26}$$

It is straightforward to obtain the relationships [23]

$$m^1 = f\frac{\Gamma_1(\Sigma^0_+) - \Gamma_1(\Sigma^0_-)}{\Sigma^0_+ - \Sigma^0_-},$$

$$\Sigma^1_\pm = \frac{m^1/f - \Gamma_1'(\Sigma^0_\pm)}{1/f + F_0''(\Sigma^0_\pm)}. \tag{7.27}$$

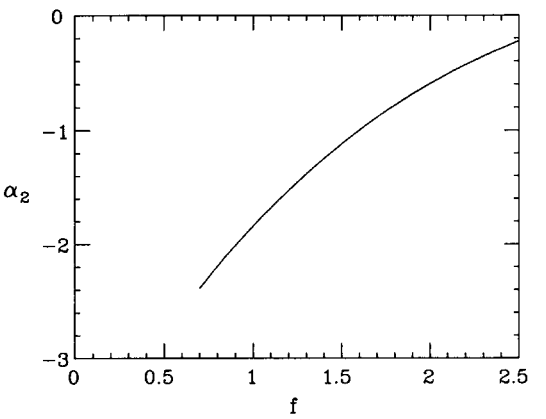

Fig. 11. The multiplicative renormalization coefficient $\alpha_2(f)$.

In the small-coupling region we can ignore the irrelevant operators and evaluate, by the use of eq. (7.16)

$$\Gamma_1(\Sigma_\pm^0) \approx \pm\Sigma_0\left[\bar{a}_1 - \frac{\pi}{f}\bar{b}_1\right] + \tfrac{1}{2}\Sigma_0^2 G_1(t_0),$$

$$\Gamma_1'(\Sigma_\pm^0) \approx \bar{a}_1 + \bar{b}_1\left(1 - \frac{\pi}{f}\right) \pm \Sigma_0\left(\left[G_1 + \frac{1}{2}\frac{\partial G_1}{\partial t}\right]_{t=t_0} - 2\pi a_3 \bar{b}_1\right), \tag{7.28}$$

where $t_0 = -\pi/f$, and in the same approximation

$$\frac{1}{f} + F_0''(\Sigma_\pm^0) \approx \frac{1}{\pi}(1 \pm 4\pi a_3 \Sigma_0). \tag{7.29}$$

Therefore, we obtain

$$m^1 \approx f\bar{a}_1 - \pi\bar{b}_1,$$

$$\Sigma_\pm^1 \approx \mp\pi\Sigma_0\left(\left[G_1 + \tfrac{1}{2}G_1'\right]_{t=t_0} - 6\pi a_3\bar{b}_1\right) - \pi\bar{b}_1. \tag{7.30}$$

As we mentioned before, in order to compare with the continuum limit we have to subtract from $\Sigma_\pm^1$ the nonmultiplicative term $-\pi\bar{b}_1$. Therefore, the scaling part of $\Sigma_\pm^1$ is

$$\mp\pi\Sigma_0\left(\left[G_1 + \tfrac{1}{2}G_1'\right]_{t=t_0} - 6\pi a_3\bar{b}_1\right). \tag{7.31}$$

Making use of the small-Σ expansion for $\Pi(k, \Sigma)$ (7.2) in the definition of $\Gamma_1'(f, \Sigma)$ leads to the following result:

$$\left[G_1 + \tfrac{1}{2}G_1'\right]_{t=t_0} = -\frac{1}{\pi}\ln\left(\frac{2\Sigma_0}{\Lambda}\right) - \int\frac{d^2k}{(2\pi)^2}\left[\pi B_2(k) + 2\frac{\bar{k}^2 - \mathcal{M}^2(k)}{\left(\bar{k}^2 + \mathcal{M}^2(k)\right)^2}\right]$$

$$+ \frac{1}{2}\int\frac{d^2k}{(2\pi)^2}\left[\frac{2A_2 + B_2 + 2\pi B_2\Pi_0}{1/f + \Pi_0}\right.$$

$$\left. - \frac{(\pi/fB_1 - A_1)(\pi/fB_1 - B_1 - A_1)}{(1/f + \Pi_0)^2}\right], \tag{7.32}$$

where all the integrals are proper and convergent around $k = 0$.

As a consequence, the nonperturbative part of $\Sigma^1_\pm$ is

$$\pm\Sigma_0\left(-\frac{\pi}{f}+\bar{a}_2(f)\right), \tag{7.33}$$

where $\bar{a}_2(f)$ is a series expandable (non-Borel-summable) function of f, nonsingular in the small-coupling region, and

$$\bar{a}_2(0)=\ln 2+\tfrac{1}{2}+2\pi\int\frac{\mathrm{d}^2k}{(2\pi)^2}\,\frac{\mathscr{M}^2(k)}{\left(\bar{k}^2+\mathscr{M}^2(k)\right)^2}, \tag{7.34}$$

is the $O(1/N)$ correction to the Λ parameter in the lattice regularization scheme. Numerically, for $r_2=\frac{1}{3}$, we have

$$\bar{a}_2(0)=1.65400, \qquad \bar{a}_2'(0)=-0.46722. \tag{7.35}$$

Eq. (7.33) is in agreement with the analysis presented in sect. 3, as required by the universality of the renormalization-group coefficients in the two-loop approximation. In particular, no logarithmic dependence on f is present, in contrast with ref. [23].

In table 3 the values of m^1 and $\Sigma^1_\pm$ corresponding to the large-N solutions of table 1 are presented; they are obtained by numerical evaluation of the exact eqs.

TABLE 3
$O(1/N)$ corrections to critical mass and condensate, as given by eq. (7.27)

f	Σ^1_+	Σ^1_-	m^1
2.5	0.42038	0.70243	0.485286
2.4	0.40110	0.68637	0.471446
2.3	0.38118	0.66978	0.457279
2.2	0.36063	0.65257	0.442757
2.1	0.33945	0.63464	0.427851
2.0	0.31769	0.61586	0.412528
1.9	0.29543	0.59609	0.396754
1.8	0.27278	0.57518	0.380496
1.7	0.24996	0.55293	0.363714
1.6	0.22722	0.52913	0.346379
1.5	0.20497	0.50352	0.328457
1.4	0.18371	0.47585	0.309932
1.3	0.16411	0.44581	0.290783
1.2	0.14688	0.41306	0.271001
1.1	0.13287	0.37758	0.250656
1.0	0.12268	0.33917	0.229763
0.9	0.11658	0.29808	0.208398
0.8	0.11400	0.25501	0.186650

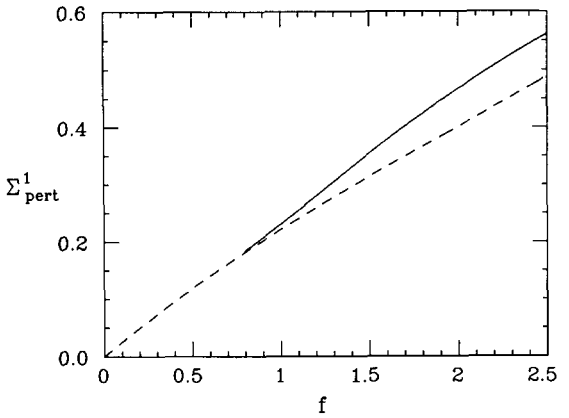

Fig. 12. The $1/N$ perturbative contribution to Σ, $\frac{1}{2}(\Sigma^1_+ + \Sigma^1_-)$ (solid line), compared with $-\pi\bar{b}_1$ (dashed line).

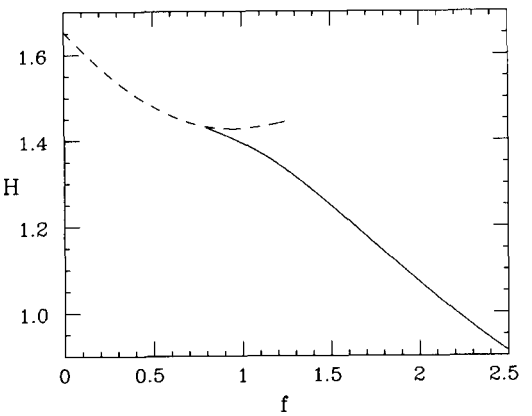

Fig. 13. The nonuniversal contribution to the nonperturbative part of Σ^1, $H = (\Sigma^1_+ - \Sigma^1_-)/(2\Sigma_0) + \pi/f$, obtained by numerical evaluation of eq. (7.27) (solid line), compared with $\bar{a}_2$, obtained by numerical integration of eq. (7.32) (dashed line).

(7.27). The perturbative contribution to Σ^1 is compared with $-\pi\bar{b}_1$ in fig. 12. The nonperturbative part is compared in fig. 13 with $\bar{a}_2$, resummed up to $O(\exp(-2\pi/f))$ by the method described in appendix A.

8. The Monte Carlo simulation

The purpose of our Monte Carlo simulation is essentially twofold:

(i) we want to check the possibility of establishing by numerical simulation the critical value of the bare mass m_c corresponding to the restoration of the chiral (γ_5) invariance in presence of an explicit breakdown of this symmetry;

(ii) we want to determine the expectation value of physical quantities at the critical point and compare the numerical extrapolations $\delta\Sigma \to 0$ and $n_{\rm pf} \to \infty$ to the known theoretical predictions.

Such an analysis offers us a possibility to discuss the feasibility and reliability of the pseudofermion method, and to evaluate quantitatively, with properly designed tests, the effects of the systematic errors discussed in sect. 2.

As we mentioned before, at the critical value of the bare mass, corresponding to the continuum limit $m_{\rm ren} = 0$, a first-order phase transition takes place. It is therefore natural to search for such a transition by performing hysteresis cycles in which we measure the vacuum expectation value of Σ versus different values of m at fixed coupling constant f. The coordinates of the center of the hysteresis cycle correspond to the location of the critical point and to the value of the perturbative contribution to the fermion condensate, defined by the relationship (holding at the critical point) [23]

$$\langle \Sigma \rangle_{\pm} = \langle \Sigma \rangle_{\rm pert} \pm \langle \Sigma \rangle_{\rm nonpert} . \tag{8.1}$$

Since this determination is somehow inaccurate, the method is refined by exploring the central region of the cycle by the *mixed-phase* technique. The starting configuration is obtained by assigning the "positive vacuum" value to half of the sites of the lattice, and the "negative vacuum" value to the other half. Thermalization tends to bring the whole lattice into the lower energy vacuum, this one being the positive one for $m > m_{\rm c}$ and the negative one for $m < m_{\rm c}$. At the critical mass, the lattice evolves into a metastable mixed-phase configuration ("soliton–antisoliton") and the average value $\langle \Sigma \rangle$ is left at its perturbative value $\frac{1}{2}(\Sigma_+ + \Sigma_-)$.

Once the critical mass has been determined, simulations are performed both in the positive and in the negative phase in order to evaluate accurately the expectation values of physical quantities. Of special interest is the non-perturbative contribution to the expectation value of Σ, that is the value of the fermion condensate $\langle \bar{\psi}\psi \rangle$

$$\langle \Sigma \rangle_{\rm nonpert} = \tfrac{1}{2}(\Sigma_+ - \Sigma_-) . \tag{8.2}$$

Another very important quantity is the value of the connected part of the composite operator $\Sigma^2(x)$, defined in eq. (7.8) and measuring the variance of the field, i.e. the steepness of the potential well.

As observed in sect. 2, a crucial parameter in the simulation is the average square of the step size in the bosonic field update $\langle (\delta\Sigma)^2 \rangle$. Therefore, the mixed, negative and positive start simulations discussed above must be repeated for different values of $\langle (\delta\Sigma)^2 \rangle$, leading to systematically different values for the measured quantities, $m_{\rm c}$ itself included.

In the optimistic view, one should be able to discover a linearity region in the dependence of the physical quantities from $\langle (\delta\Sigma)^2 \rangle$, for sufficiently small $\langle (\delta\Sigma)^2 \rangle$, and therefore to extrapolate linearly down to $\langle (\delta\Sigma)^2 \rangle \to 0$.

In our view, the reliability of these extrapolations partly rests on the crucial test we mentioned in sect. 2, i.e. the linear dependence on $\langle(\delta\Sigma)^2\rangle$ and extrapolation to zero of the quantum Schwinger–Dyson equations

$$\Delta\left\langle \frac{\delta S}{\delta \Sigma} \right\rangle \to 0. \tag{8.3}$$

We must also take into account the dependence of the numerical results on the number n_{pf} of pseudofermion sweeps used to compute K^{-1}. The statistical error $O(1/\sqrt{n_{\mathrm{pf}}})$ affecting the inversion procedure turns into a systematic error $O(1/n_{\mathrm{pf}})$ in the expectation values of physical quantities.

The statement can be made more quantitative if we assume eq. (2.8) to hold and the matrix ε to be independent of the field configuration. The effective action of the model can then be modified to account for the introduced noise by

$$S \to S - N\varepsilon \sum_x \eta(x)\Sigma(x), \tag{8.4}$$

where we have parametrized $\operatorname{tr}\varepsilon(x, x) = \varepsilon\eta(x)$, $\eta(x)$ being a normalized gaussian noise and ε an experimentally determined parameter. In the range of values $N \geqslant 10$, $f = 1.8$–2.2 the numerical analysis performed at the critical point gives

$$\varepsilon \cong \frac{1.2}{\sqrt{n_{\mathrm{pf}}}}. \tag{8.5}$$

A straightforward computation to lowest order in ε shows that, using standard lattice averaging procedures,

$$\langle\Sigma\rangle \to \langle\Sigma\rangle + \tfrac{1}{2}\varepsilon^2\left(N^2\langle\Sigma^3\rangle_{\mathrm{c}}\right), \tag{8.6}$$

$$\langle\Sigma^2\rangle_{\mathrm{c}} \to \langle\Sigma^2\rangle_{\mathrm{c}} + \varepsilon^2\left[\left(N\langle\Sigma^2\rangle_{\mathrm{c}}\right)^2 + \frac{1}{2N}\left(N^3\langle\Sigma^4\rangle_{\mathrm{c}}\right)\right]. \tag{8.7}$$

Recalling the well known property of the $1/N$ expansion

$$\langle\Sigma^n\rangle_{\mathrm{c}} \sim N^{-n+1}, \tag{8.8}$$

we find that the systematic error due to pseudofermionic noise is depressed by a factor $1/n_{\mathrm{pf}}$ in $\langle\Sigma\rangle$ and only by a factor N/n_{pf} in $\langle\Sigma^2\rangle_{\mathrm{c}}$.

9. Details of the computation

The simulation algorithm is dominated by the inversion of $K^\dagger K$, both from the point of view of complexity and of computation amount.

For the Symanzik-improved theory, $K^\dagger K$ involves interactions up to the fourth neighbour. To allow for the parallel upgrading of the pseudofermion fields χ, we divided the lattice sites into ten "colors", the sites of the same color being uncorrelated by $K^\dagger K$. All the χ fields belonging to the same color are updated simultaneously, using the heat-bath algorithm.

On the other hand, the updating of the bosonic fields Σ that is performed using the Metropolis algorithm is very easy, since the variation (2.5) of the effective action does not involve correlations of Σ at different sites.

The Schwinger–Dyson equations (2.10) of the Gross–Neveu model have the form

$$\left\langle \operatorname{Tr} K^{-1}(x,x) \right\rangle = \frac{1}{N} \left\langle \frac{\delta S_b}{\delta \Sigma(x)} \right\rangle , \tag{9.1}$$

where the right-hand side is a simple polynomial in $\Sigma(x)$. To check the accuracy of eq. (9.1), we measure the two quantities after each iteration. The left-hand side is computed as a part of the Monte Carlo inversion.

The computation was implemented in a FORTRAN code for a CRAY XMP computer. One iteration on a 40×40 lattice, including 100 upgradings of the χ's and one of the Σ's, is performed in 0.45 CPU s, 95% of which are spent in the computation of the matrix elements of K^{-1}.

10. Numerical results

We selected several values of the coupling constant f in the scaling region; for each f, the simulation was performed on a $L \times L$ lattice, with antiperiodic bound-

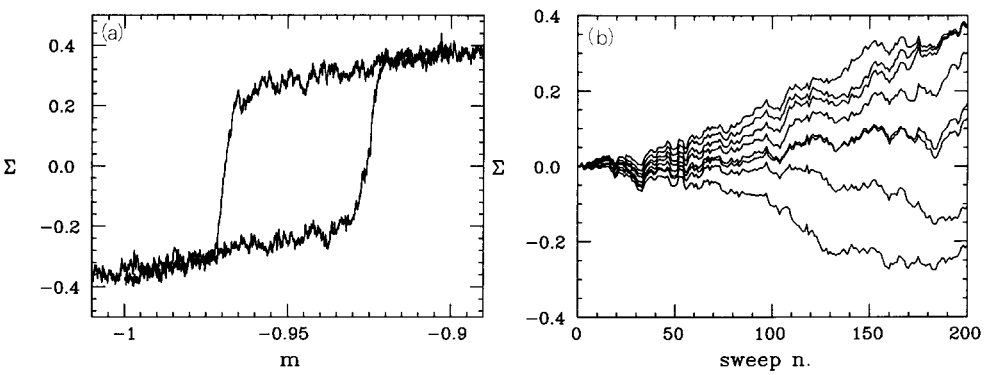

Fig. 14(a). Thermal cycle for $N = 10$, $f = 2.0$ and $\langle (\delta\Sigma)^2 \rangle = 0.0093$. (b) Mixed phase runs for $N = 10$, $f = 2.0$ and $\langle (\delta\Sigma)^2 \rangle = 0.0093$. The curves correspond, from top to bottom, to the masses $m = -0.940$, -0.942, -0.944, -0.946, -0.948, -0.949, -0.950 and -0.952. m_c is estimated to be -0.949 ± 0.001.

ary conditions, choosing L large enough to have small ($O(10^{-5})$) finite-size corrections (this is obtained by choosing $S \simeq 12$, cf. sect. 6).

The simulation starts with the determination of the critical mass m_c. It was first estimated by a thermal cycle and then, more precisely, by mixed-phase runs. We required a precision of 0.001 in the determination of m_c. The physical observables and $\delta S/\delta\Sigma$ were then measured at m_c in the two phases, starting from the "positive" configuration $\Sigma(x) = \Sigma_+$ and from the "negative" one $\Sigma(x) = \Sigma_-$. The whole procedure was repeated for several values of $\langle(\delta\Sigma)^2\rangle$. When a previous run at different $\langle(\delta\Sigma)^2\rangle$allowed for an estimate of m_c, we skipped the thermal cycle but we always recomputed m_c by mixed-phase runs for each $\langle(\delta\Sigma)^2\rangle$.

The results were then extrapolated to $\langle(\delta\Sigma)^2\rangle \to 0$ with a linear fit, and compared with the $O(1/N)$ analytical results. We used values of $\langle(\delta\Sigma)^2\rangle \approx 0.002$–$0.02$, corresponding to acceptances ≈ 80–95%. n_{sw}, the number of sweeps used to measure the observables, was rescaled keeping $\langle(\delta\Sigma)^2\rangle n_{sw}$ constant. Typical values of n_{sw} run from 200 for $\langle(\delta\Sigma)^2\rangle \approx 0.02$ to 2000 for $\langle(\delta\Sigma)^2\rangle \approx 0.002$. Typical examples of a thermal cycle and of a mixed phase run are presented in fig. 14.

For $N = 10$ and $n_{pf} = 100$, we investigated $f = 1.6$, $L = 60$, $f = 1.8$, $L = 50$, $f = 2.0$, $L = 40$ and $f = 2.2$, $L = 40$. We checked that $n_{pf} = 200$ gives similar results.

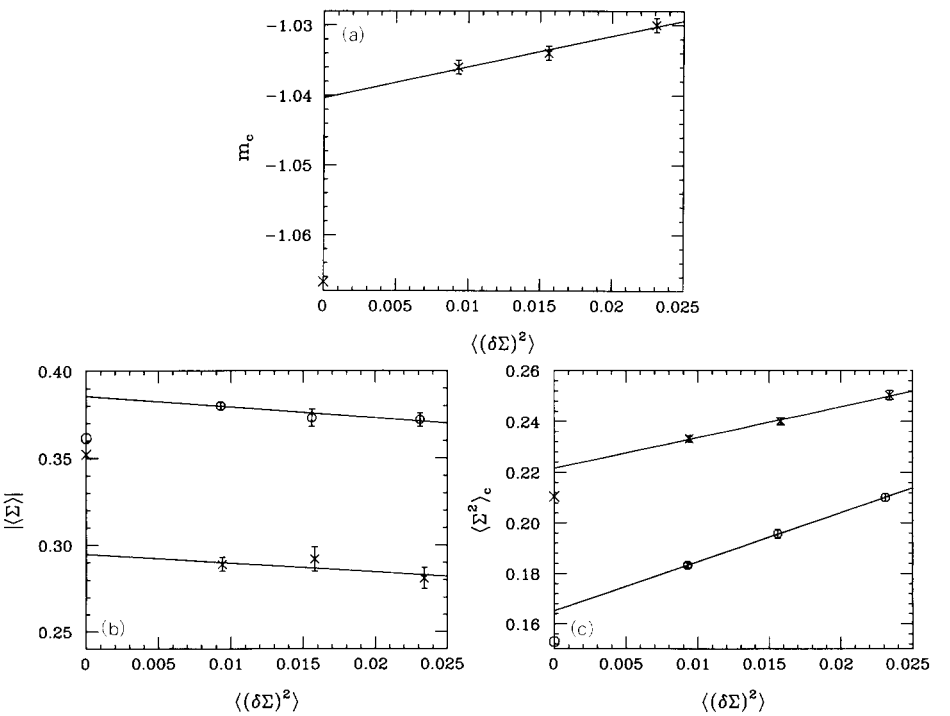

Fig. 15(a). The critical mass m_c for $N = 10$, $n_{pf} = 100$ and $f = 2.2$. (b) $\langle\Sigma\rangle$ for $N = 10$, $n_{pf} = 100$ and $f = 2.2$. (c) $\langle\Sigma^2\rangle_c$ for $N = 10$, $n_{pf} = 100$ and $f = 2.2$. ○: positive phase data; ×: negative phase data.

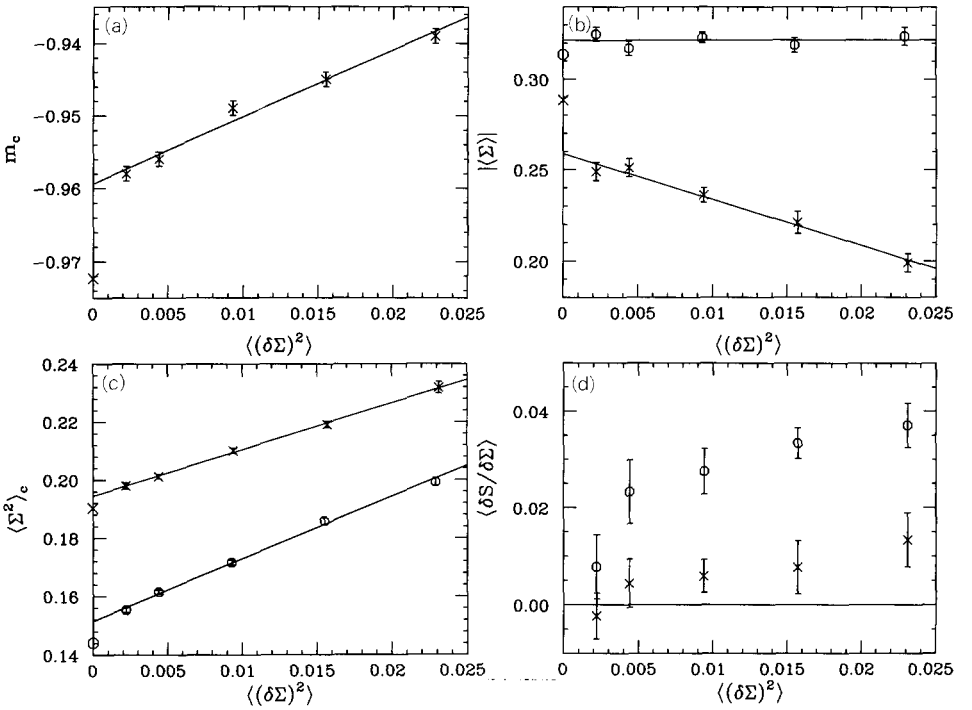

Fig. 16. (a) m_c; (b) $\langle\Sigma\rangle$; (c) $\langle\Sigma^2\rangle_c$; and (d) the value of the Schwinger–Dyson equation. In all cases $N = 10$, $n_{pf} = 100$, and $f = 2.0$.

Numerical results for m_c, $\langle\Sigma\rangle$ and $\langle\Sigma^2\rangle_c$ in the two phases are presented in figs. 15–18. The straight lines are the results of a linear fit in $\langle(\delta\Sigma)^2\rangle$; as discussed in sects. 2 and 8, the numerical estimate of the observables is given by the extrapolation of the fit to $\langle(\delta\Sigma)^2\rangle = 0$. We plotted for comparison at $\langle(\delta\Sigma)^2\rangle = 0$ the results of the $1/N$ expansion up to $O(1/N)$.

These three quantities are remarkably linear in $\langle(\delta\Sigma)^2\rangle$. The two points at very small $\langle(\delta\Sigma)^2\rangle$, that we computed for $f = 2.0$, stabilize the extrapolation to $\langle(\delta\Sigma)^2\rangle \to 0$, but do not change dramatically the result. Numerical results for m_c and $\langle\Sigma_{\pm}\rangle$ do not seem to extrapolate to the theoretical results, even allowing for an $O(1/N^2)$ uncertainty; on the other hand, the extrapolation of $\langle\Sigma^2\rangle_c$ looks compatible with the $1/N$ computation.

The value of the Schwinger–Dyson equation $\langle\delta S/\delta\Sigma\rangle$ is shown only for $f = 2.0$, in fig. 16d; it is very similar for the other values of f. Its behavior is not linear, but possibly for the two leftmost points. We investigated also the case $N = 30$, $f = 2.0$ for $L = 40$; results are presented in fig. 19 for $n_{pf} = 100$ and in fig. 20 for $n_{pf} = 300$ (in these figures the linear fits are performed only on the three left-most points).

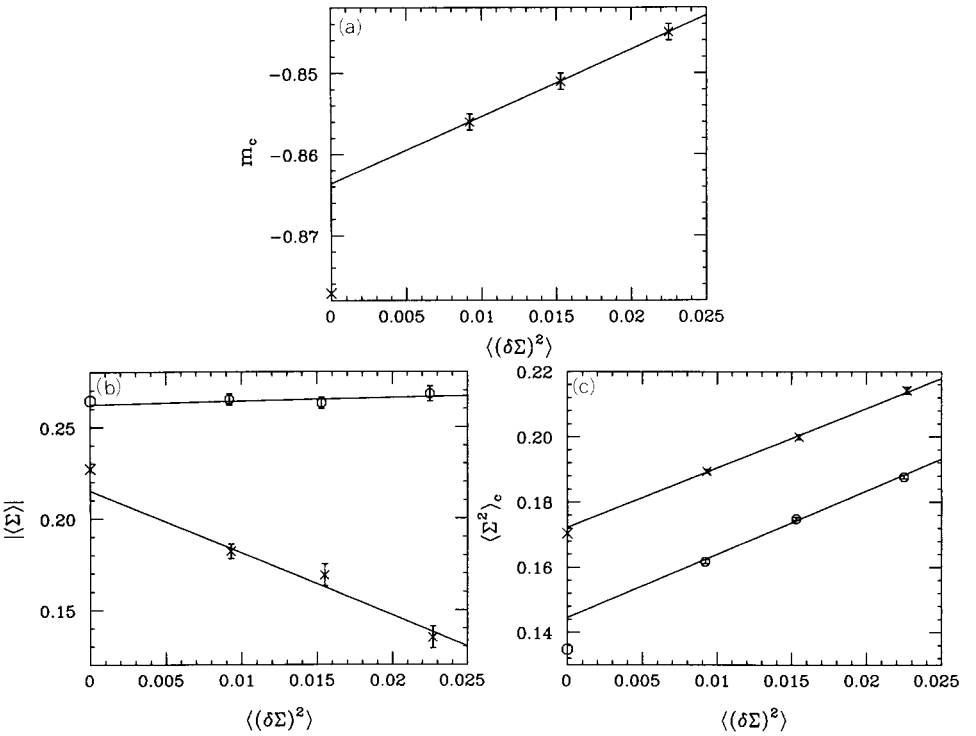

Fig. 17. (a) m_c; (b) $\langle\Sigma\rangle$; (c) $\langle\Sigma^2\rangle_c$. In all cases $N = 10$, $n_{pf} = 100$, and $f = 1.8$.

In this case, we see a clear difference between different n_{pf}'s; in particular, $n_{pf} = 300$ data show a milder dependence on $\langle(\delta\Sigma)^2\rangle$. This was to be expected, since quantum fluctuations are $O(1/N)$ and therefore the relevance of pseudo-fermion-induced fluctuations (independent of N but dependent on n_{pf}) is growing with growing N. Also the Schwinger–Dyson equation shows a much higher expectation value for $N = 30$ than for $N = 10$ (at the same n_{pf} and $\langle(\delta\Sigma)^2\rangle$), indicating the need for a bigger n_{pf}.

We can estimate the effect on the other observables of an error in the critical mass Δm_c in the following way: in the set of eqs. (5.8), the first equation $\Gamma_0(\Sigma_+) = \Gamma_0(\Sigma_-)$ is violated by the incorrect determination of m_c; let us assume that the numerical algorithm works properly in the positive and negative phases, and therefore the second equation $\delta\Gamma_0(\Sigma_\pm)/\delta\Sigma = 0$ is satisfied. The leading contribution to $\Delta\Sigma_\pm$, the error induced by Δm_c on $\langle\Sigma_\pm\rangle$, is computed from

$$\Delta m_c \frac{\partial \Gamma_0'}{\partial m} + \Delta\Sigma_\pm \Gamma_0'' = 0,$$

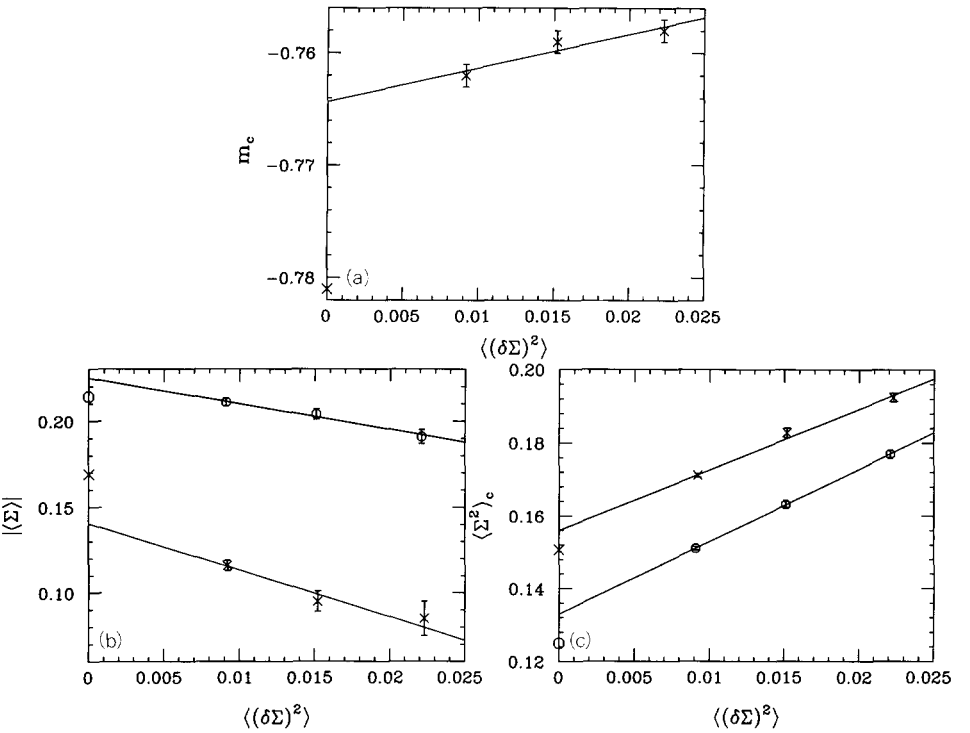

Fig. 18. (a) m_c; (b) $\langle\Sigma\rangle$; (c) $\langle\Sigma^2\rangle_c$. In all cases $N = 10$, $n_{pf} = 100$, and $f = 1.6$.

with

$$\frac{\partial\Gamma_0'}{\partial m} = -\frac{1}{f} \quad \text{and} \quad \Gamma_0'' = \frac{1}{\pi}(1 \pm 4\pi a_3\Sigma_0) + O(\Sigma_0^2), \tag{10.1}$$

where the prime stands for derivative respect to Σ and all the derivatives are evaluated at $m = m_c$ and $\Sigma = \Sigma_\pm$; the result is

$$\Delta\Sigma_\pm \simeq \Delta m_c \frac{\pi}{f}(1 \mp 4\pi a_3\Sigma_0). \tag{10.2}$$

Using eq. (7.22), we find for the error on $\langle\Sigma^2\rangle_c$

$$\Delta\langle\Sigma^2\rangle_c \simeq \Delta\Sigma \frac{1}{N}\frac{\partial C_1}{\partial\Sigma} \simeq \frac{\Delta\Sigma_\pm}{N}[\alpha_1(f) + 2\alpha_2(f)\Sigma_\pm], \tag{10.3}$$

and, since $|\alpha_1| < 1$ and $|\alpha_2| < 1$ in the relevant range of values of f, $\Delta\langle\Sigma^2\rangle_c$ is negligible.

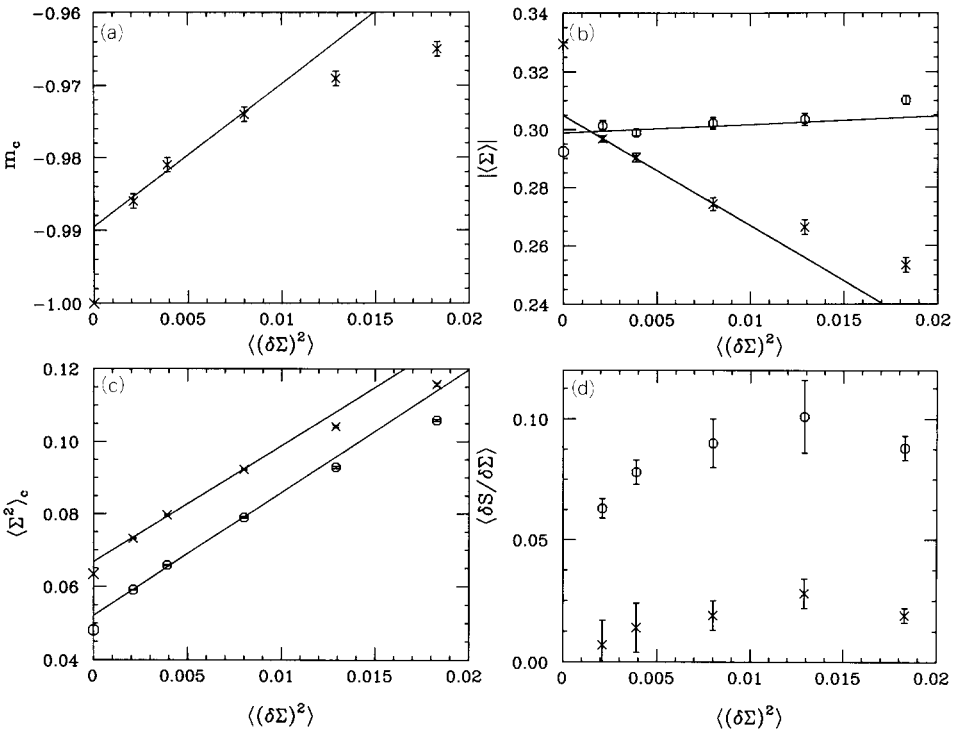

Fig. 19. (a) m_c; (b) $\langle\Sigma\rangle$; (c) $\langle\Sigma^2\rangle_c$; and (d) the value of the Schwinger–Dyson equation. In all cases $N = 30$, $n_{pf} = 100$, and $f = 2.0$.

The observed values of Δm_c and the corresponding computed values of $\Delta\Sigma_{\pm}$ are listed in table 4. We note that these values account for most of the deviations from theoretical predictions.

11. Conclusions and outlook

We think that the achieved theoretical status of the lattice Gross–Neveu model in the large-N limit is fully satisfactory up to $O(1/N)$. Every observable (in the sense of statistical mechanics) is unambiguously calculable and the continuum limit is well defined and coincides with the field-theoretical predictions.

Problems related to the non-Borel summability of perturbative series can be solved by defining computational procedures such that every relevant number can be obtained with aribtrary precision, as shown in appendix A. We also put under control finite-volume dependences, which allowed us to quantify the effect of Symanzik improvement.

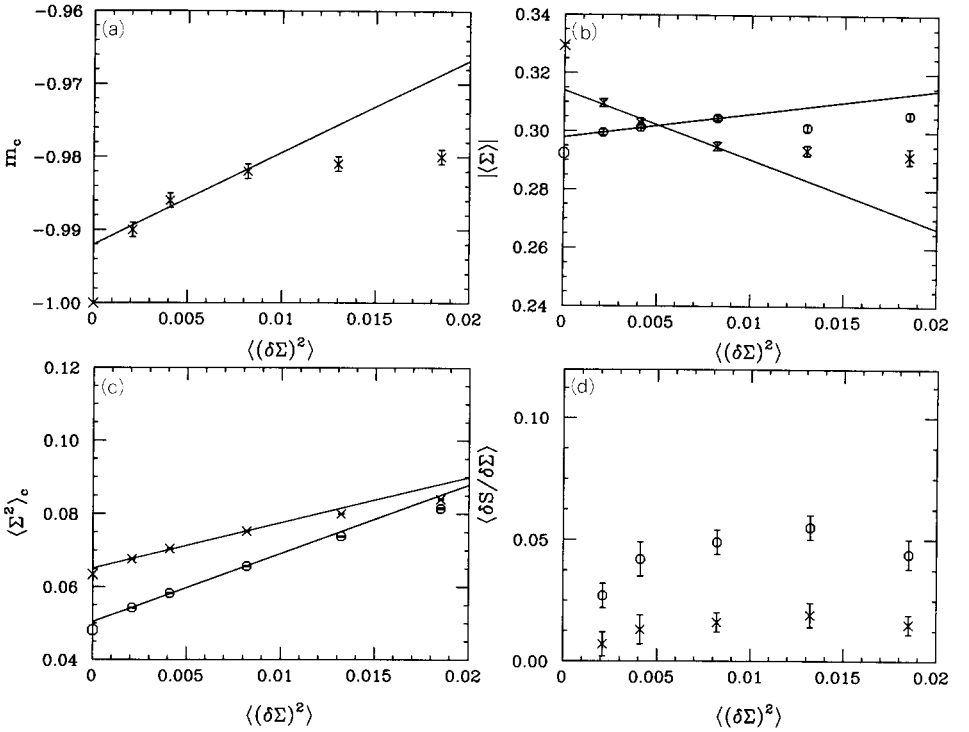

Fig. 20. (a) m_c; (b) $\langle\Sigma\rangle$; (c) $\langle\Sigma^2\rangle_c$; and (d) the value of the Schwinger–Dyson equation. In all cases $N = 30$, $n_{pf} = 300$, and $f = 2.0$.

TABLE 4
The error on the determination of the critical mass Δm_c and the induced errors $\Delta\Sigma_+$ and $\Delta\Sigma_-$ relative to the data presented in figs. 15–20

Fig. n	f	Δm_c	$\Delta\Sigma_+$	$\Delta\Sigma_-$
15	2.2	0.027	0.028	0.049
16	2.0	0.013	0.016	0.025
17	1.8	0.013	0.018	0.027
18	1.6	0.017	0.028	0.038
19	2.0	0.010	0.012	0.019
20	2.0	0.008	0.010	0.015

The analysis of the Monte Carlo data showed that the pseudofermion method is not very efficient in the large-N limit of the Gross–Neveu model. In particular, while the error induced by Monte Carlo inversion of the fermion propagator can be kept under control, the dependence on $\langle(\delta\Sigma)^2\rangle$ is only poorly understood. This is essentially due to a lack of theoretical understanding on the violation of the Schwinger–Dyson equations induced by $\langle(\delta\Sigma)^2\rangle$, which spoils the efficiency of this conceptually simple and conclusive test.

The extrapolation of the numerical results to zero upgrading step show small but systematic deviations from the theoretical predictions. These deviations are accounted for by the imprecise determination of the critical mass, as discussed in detail in sect. 10. Anyway, one firm result of our analysis is the capability of the pseudofermion method of dealing with spontaneous breakdown of symmetries, at least in the discrete case.

We must mention that the problem we faced refers to the worst possible dependence on approximations for the Matthews–Salam determinant, that of a purely fermionic theory with a large number of degrees of freedom. Most interesting physical models should have a less critical dependence. This statement includes supersymmetric models, where fermions are balanced by an equal number of bosons, and the extremely favorable case of QCD, where there are $\sim N$ times as many bosons as fermions and the quenched approximation appears to work. In these models we expect the pseudofermion method to be more efficient, since it deals exactly with bosonic degrees of freedom.

These conclusions seem to indicate several possible directions of future research. We would like to extend our analysis to continuous symmetries, with special regard to the lattice implementation of chirality and supersymmetry [34]. It would be interesting to compare the mass spectra of semiclassically solvable models with their lattice counterparts. In the context of numerical analysis, two open questions seem to be most relevant. It would be necessary to have a theoretical prediction of the small $\langle(\delta\Sigma)^2\rangle$ dependence of measured quantities and in particular to know the coefficient of the linear term in the violation of the Schwinger–Dyson equations. We would also like to compare our results with those obtained with different methods, with a special interest for the competing Langevin method.

Appendix A

The problem of an explicit and unambiguous evaluation of the continuum (nonperturbative) part of quantum operators carrying no nontrivial quantum numbers can be explicitly addressed in the Gross–Neveu model by considering the quantity $\langle\Sigma^2(x)\rangle_c$ defined in eq. (7.8).

The lattice value of this operator can be computed (in the $1/N$ expansion) from eq. (7.9), which requires subtraction of a perturbative tail whose formal definition,

resulting from eq. (7.10), is given in terms of

$$C_1(f,0) \equiv \int \frac{\mathrm{d}^2k}{(2\pi)^2} \frac{1}{1/f + \Pi_0(k)} = \sum_{n=0}^{\infty} (-1)^n c_n f^{n+1}, \tag{A.1}$$

$$c_n = \int \frac{\mathrm{d}^2k}{(2\pi)^2} [\Pi_0(k)]^n \underset{n\to\infty}{\longrightarrow} \frac{\Lambda^2}{4\pi} (-1)^n \frac{n!}{(2\pi)^n}. \tag{A.2}$$

The series (A.1) is not Borel summable, but we claim that a summation procedure can be defined in such a way that its result reproduces the numerical value of the integral for every value of f to any desired precision.

More precisely, since we could not find any direct numerical algorithm for the evaluation of the integral, because of the singularity of the integrand due to the vanishing of the denominator when $k \approx \Sigma_0(f)$, we computed its value through the relationship (7.10)

$$C_1(f,0) = -2f^2 \frac{\partial}{\partial f} \Gamma_1(f,0), \tag{A.3}$$

where

$$\Gamma_1(f,0) \equiv \frac{1}{2} \int \frac{\mathrm{d}^2k}{(2\pi)^2} \ln\left[\frac{1}{f} + \Pi_0(k)\right] = -\tfrac{1}{2} \ln f + \sum_{n=1}^{\infty} \frac{(-1)^{n+1}}{2n} c_n f^n \tag{A.4}$$

can be easily evaluated numerically. Eq. (A.3) allows us to focus on the evaluation of $\Gamma_1(f,0)$; most of the discussion will, however, apply directly to C_1 as well as to Γ_1.

Central to our analysis is the observation that the integral (and the series as well) can be splitted into two domains, the region $|k| < \Lambda$ and the region $|k| > \Lambda$, and that integration in the external region shows no pathology, while the corresponding series defined by the coefficients

$$c_n^{\mathrm{ext}} = \int_{|k|>\Lambda} \frac{\mathrm{d}^2k}{(2\pi)^2} [\Pi_0(k)]^n \tag{A.5}$$

is summable in the standard sense and therefore brings an unambiguous contribution to the final result. For the sake of it, we estimated the convergence radius of the external contribution from explicit evaluation of the first 20 coefficients and found it to be

$$f_{\mathrm{conv}} \approx 3.6 \approx [\Pi_0^{\max}]^{-1}. \tag{A.6}$$

We are therefore left with the task of resumming the series defined by

$$c_n^{\text{int}} = \int_{|k|<\Lambda} \frac{\mathrm{d}^2 k}{(2\pi)^2} [\Pi_0(k)]^n . \tag{A.7}$$

Let us observe that, in the relevant region, $\Pi_0(k)$ can be represented by its expansion in a series of the lattice spacing a

$$\Pi_0(k) = \frac{1}{2\pi} \ln\left(\frac{k^2}{\Lambda^2}\right) + \Delta_2 a^2 k^2 + \sum_{m=2}^{\infty} a^{2m} \sum_{l=0}^{[m/2]} \left(\Delta_{2m,l} + \Delta'_{2m,l} \ln\left(\frac{k^2}{\Lambda^2}\right)\right) P_{2m,l}(k), \tag{A.8}$$

where $P_{2m,l}(k)$ are the independent orthogonal polynomials of degree $2m$ in k_x, k_y enjoying the symmetries

$$k \leftrightarrow -k, \qquad k_x \leftrightarrow k_y . \tag{A.9}$$

In particular

$$P_{2m,0} = (k^2)^m, \qquad P_{2m,1} = (k^2)^{m-2} \left[4 \sum_{\mu} k_\mu^4 - 3(k^2)^2\right]. \tag{A.10}$$

This representation of $\Pi_0(k)$ allows for the analytical integration of the coefficients c_n^{int} with a precision that is only related to our ability in computing the coefficients $\Delta_{2m,l}$ and $\Delta'_{2m,l}$. Appendix B is devoted to this problem. By observing that (choosing $x = k^2/\Lambda^2$)

$$\int_0^1 x^m \ln^n x \, \mathrm{d}x = (-1)^n \frac{n!}{(m+1)^{n+1}}, \tag{A.11}$$

we recognize that the expansion (A.8), once substituted in eq. (A.7), leads unambiguously to the representation

$$c_n^{\text{int}} = \frac{\Lambda^2}{4\pi} (-1)^n \frac{n!}{(2\pi)^n} \left[1 + \sum_{m=1}^{\infty} \frac{d_m}{(m+1)^n}\right], \tag{A.12}$$

where d_m can be analytically determined as functions of $\Delta_{2m,l}$ and $\Delta'_{2m,l}$ and must possibly be set of zero for a finite set of values of $n < m$.

Our resummation simply consists in replacing c_n^{int} with its representation (A.12), thus obtaining a sum of series whose general form is

$$\sum_{n=0}^{\infty} n! \left[\frac{f}{2\pi(m+1)} \right]^{n+1}, \tag{A.13}$$

times coefficients depending on Λ and d_m. Now the series

$$\sum_{n=0}^{\infty} n! x^{n+1} \tag{A.14}$$

is the asymptotic expansion of the well-known function

$$\exp\left(-\frac{1}{x}\right) \mathrm{Ei}\left(\frac{1}{x}\right) = -\mathrm{Re} \int_0^1 \ln(1 + x \ln t)\, \mathrm{d}t, \tag{A.15}$$

and therefore our internal integral can be re-expressed in the form of an infinite sum over exponential–integral functions of increasing argument.

Resumming only the series for $m \leqslant m_0$ and replacing the rest with a standard (non-resummed) series leads to an error $\mathrm{O}(\exp(-2\pi(m_0+2)/f))$, that can evidently be made as small as desired by a proper choice of m_0. An explicit evaluation of Γ_1^{int} up to $m_0 = 2$ leads to

$$\begin{aligned} \Gamma_1^{\mathrm{int}} \approx -\frac{\Lambda^2}{8\pi} \Bigg\{ & \ln f + \exp\left(-\frac{2\pi}{f}\right) \mathrm{Ei}\left(\frac{2\pi}{f}\right) - 2\pi\Lambda^2 \Delta_2 \exp\left(-\frac{4\pi}{f}\right) \mathrm{Ei}\left(\frac{4\pi}{f}\right) \\ & + \tfrac{3}{2}\left(2\pi\Lambda^2\Delta_2\right)^2 \left[\exp\left(-\frac{6\pi}{f}\right) \mathrm{Ei}\left(\frac{6\pi}{f}\right) - \frac{f}{6\pi} \right] \\ & - 2\pi\Lambda^4 \Delta_{4,0} \exp\left(-\frac{6\pi}{f}\right) \mathrm{Ei}\left(\frac{6\pi}{f}\right) \Bigg\}. \end{aligned} \tag{A.16}$$

Comparison of results in the form (A.16) extended to higher orders with explicit numerical integration of Γ_1^{int} on big lattices ($L = 300$) leads to extremely satisfactory results up to $f = 3.0$, showing the essential accuracy of the resummation scheme and leading to our theoretical predictions for $C_1(f, 0)$.

In order to qualify our assertions, we must specify that we do not pretend we have found a more powerful resummation scheme than Borel's. The ambiguity corresponding to the singularity in the Borel variable is still there and manifests itself through the appearance of an $\mathrm{O}(\exp(-1/x))$ imaginary part in the direct

computation of the integral (A.15), giving rise to the relationship (7.14)

$$\operatorname{Im} \Gamma_1(f,0) = \tfrac{1}{8}\Sigma_0^2 + \mathrm{O}(\Sigma_0^4). \tag{A.17}$$

Our claim is rather a statement of the irrelevance of this ambiguity in the evaluation of the integral related to C_1

$$\int_0^1 \frac{x}{1 + x \ln t}\, \mathrm{d}t, \tag{A.18}$$

for which a principal-part prescription eliminates the imaginary part. We are thus left with a calculable quantity whose value *is* well approximated both by our resummation scheme and by direct numerical computation, and represents the *uniquely defined* perturbative tail that must be subtracted in order to obtain the physical quantum expectation value.

Appendix B

Knowledge of the small-a expansion of the one-loop integral

$$\Pi_0(k) = 2 \int \frac{\mathrm{d}^2 p}{(2\pi)^2} \frac{\mathscr{M}(l_1)\mathscr{M}(l_2) - \bar{l}_1 \cdot \bar{l}_2}{\left[\bar{l}_1^2 + \mathscr{M}(l_1)^2\right]\left[\bar{l}_2^2 + \mathscr{M}(l_2)^2\right]}, \tag{B.1}$$

where $l_1 = p$ and $l_2 = p + k$, is explicitly required both in the context of the one-loop Symanzik-improvement scheme and for the purpose of resumming the $\mathrm{O}(1/N)$ perturbative contributions to physical quantities, as discussed in appendix A.

The general form of the expansion will be as in eq. (A.8). Let us just notice that, by introducing polar coordinates on the k plane, we can express the orthogonal polynomials $P_{2m,l}(k)$ in the form

$$P_{2m,l}(k) = (k^2)^m \cos(4l\theta). \tag{B.2}$$

The coefficients $\Delta_{2m,l}$ and $\Delta'_{2m,l}$ of the small-a expansion can be systematically computed by a technique exploiting dimensional continuation.

We shall not belabour on this point, already well discussed in the literature [25]. Suffice it to mention that $\Pi_0(k)$ may be expressed as the limit for $d \to 2$ of the sum of two d-dimensional integrals; the first integral is computed by expanding the integrand in powers of a and extending the integration to infinity, while the second corresponds to expanding the integrand in powers of k and integrating on the lattice. UV divergencies of the first and IR divergencies of the second integral must match to give a finite result.

In order to perform the lattice integration, one has to isolate and subtract the IR singularities, which can be done by the help of explicitly analyzable lattice integrals involving scalar propagators. We made some "technological" progress in the evaluation of such lattice integrals, which helped us in the numerical computation of the $O(a^4)$ coefficients. Since many of our results do not depend strictly on $d=2$, we report them in the following for future use and reference. The most general relevant lattice integral with no intrinsic scale is

$$J(n_k, n) = \int \frac{d^d p}{(2\pi)^d} \frac{\prod_{k=2}^{n} \left(\sum_{\mu=1}^{d} \hat{p}_\mu^{2k}\right)^{n_k}}{\left(\sum_{\mu=1}^{d} \hat{p}_\mu^2\right)^n}, \qquad \sum_{k=2}^{n} k n_k - n \leqslant 0, \tag{B.3}$$

showing an IR divergence degree

$$\omega = \tfrac{1}{2} d + \sum_{k=2}^{n} k n_k - n. \tag{B.4}$$

We can make use of the integral representation

$$\frac{1}{\left(\sum_\mu \hat{p}_\mu^2\right)^n} = \frac{1}{2^n (n-1)!} \int dz\, z^{n-1} \exp\left\{ -z \sum_{\mu=1}^{d} (1 - \cos p_\mu) \right\}, \tag{B.5}$$

and notice that

$$\int \frac{d^d p}{(2\pi)^d} \exp\left\{ -z \sum_{\mu=1}^{d} (1 - \cos p_\mu) \right\} = [u(z)]^d, \tag{B.6}$$

where $u(z)$ is related to a Bessel function and satisfies the differential equation

$$u''(z) = -\left(2 + \frac{1}{z}\right) u'(z) - \frac{1}{z} u(z). \tag{B.7}$$

Iterated use of eq. (B.7) and integration by parts allows us to express $J(n_k, n)$ in terms of the restricted set

$$J_n \equiv J(0, n) \equiv \int \frac{d^d p}{(2\pi)^d} \frac{1}{\left(\sum_\mu \hat{p}_\mu^2\right)^n} \tag{B.8}$$

by a linear relationship

$$J(n_k, n) = \sum_{m \leqslant n} \alpha_m(n_k, n, d) J_m. \tag{B.9}$$

The coefficients $\alpha_m(n_k, n, d)$ can be easily and systematically computed with the help of a symbolic manipulation program, like REDUCE. For the purpose of regularization, what we really need is the ε-expansion around D dimensions of these integrals, where $\varepsilon = d - D$. In general

$$J(n_k, n) = \frac{1}{\varepsilon} A(n_k, n) + B(n_k, n) + \mathrm{O}(\varepsilon), \tag{B.10}$$

and in particular

$$J_m = \frac{1}{\varepsilon} A_m + B_m + \mathrm{O}(\varepsilon). \tag{B.11}$$

Eq. (B.9) in turn implies that

$$A(n_k, n) = \sum_{m \leqslant n} \alpha_m(n_k, n, D) A_m,$$

$$B(n_k, n) = \sum_{m \leqslant n} \left[\frac{\partial \alpha_m(n_k, n, D)}{\partial d} A_m + \alpha_m(n_k, n, D) B_m \right]. \tag{B.12}$$

A conceptually simple trick allows us to compute all the A_m in arbitrary dimensions. The crucial observation consists in noticing that when

$$n = \sum_{k=2}^{n} k n_k, \tag{B.13}$$

the integrals are infrared finite for all D. Therefore, the following equation may be established

$$\sum_m \alpha_m\left(n_k, \sum_k k n_k, D\right) A_m = 0. \tag{B.14}$$

From this equation, one can always establish a recurrence relationship among the A_m. When $D = 2$, it takes the form

$$A_{m+1} = \frac{3m^2 - 3m + 1}{8m^2} A_m - \frac{(m-1)^2}{32m^2} A_{m-1}, \qquad A_1 = \frac{1}{2\pi}. \tag{B.15}$$

Similar considerations lead to the determination of the coefficients B_m. Direct computation of D-dimensional integrals can be in general avoided, except possibly for the first $D - 1$ among them.

In particular, when $D = 2$, it is known that

$$B_1 = \frac{1}{2\pi}\left(-\tfrac{1}{2}\ln 4\pi + \tfrac{1}{2}\gamma_E + \tfrac{5}{2}\ln 2\right), \tag{B.16}$$

and it is convenient to parametrize the integrals by

$$J_m = \frac{\bar{A}_m}{2\pi}\left[\frac{1}{\varepsilon} - \tfrac{1}{2}\ln 4\pi + \tfrac{1}{2}\gamma_E + \tfrac{5}{2}\ln 2 - \bar{C}_m\right], \tag{B.17}$$

where $\bar{A}_m$ and $\bar{C}_m$ are rational numbers. The easiest way to compute $\bar{C}_m$ is now based on the existence of the following two-dimensional identities

$$\sum_\mu \hat{p}_\mu^4 \sum_\mu \hat{p}_\mu^{2n} = 2\sum_\mu \hat{p}_\mu^{2n+4} - 2\sum_\mu \hat{p}_\mu^{2n+2}\sum_\mu \hat{p}_\mu^2 + \sum_\mu \hat{p}_\mu^{2n}\left(\sum_\mu \hat{p}_\mu^2\right)^2. \tag{B.18}$$

$\bar{C}_m$ can be determined recursively by applying (B.18) to the case of infrared finite integrals. The values of $\bar{A}_m$ and $\bar{C}_m$ for $n \leqslant 8$ are reported for reference in table 5.

Similar identities can be easily generalized to D dimensions; they are related to the properties of the representations of the permutation group for D elements. Explicit infrared singularities are not the only pathologies one can meet in evaluating higher order coefficients of the expansion of $\Pi_0(k)$. Actually, one encounters many improper integrals whose value is a finite number but whose naïve numerical evaluation on bigger and bigger square lattices leads to non-convergent results.

Typical representatives of this phenomenon are integrals in which the singularity behaviour of the integrand has the form

$$\frac{P_{2m,l}(p)}{(p^2)^n}, \qquad n > m, \qquad l > 0. \tag{B.19}$$

TABLE 5

The coefficients $\bar{A}_m$ and $\bar{C}_m$, as defined in eq. (B.16), for the lowest values of m

m	$\bar{A}_m$	$\bar{C}_m$
1	1	0
2	$\frac{1}{8}$	$\frac{1}{2}$
3	$\frac{5}{256}$	$\frac{17}{20}$
4	$\frac{7}{2048}$	$\frac{281}{252}$
5	$\frac{169}{262144}$	$\frac{16045}{12168}$
6	$\frac{269}{2097152}$	$\frac{714989}{484200}$
7	$\frac{1781}{67108864}$	$\frac{1184801}{739800}$
8	$\frac{3035}{536870912}$	$\frac{273447451}{160612200}$

In order to insure convergence of the numerical integration, these contributions must be regularized with a procedure similar to that employed with IR divergencies, but with a crucial difference related to the fact that the integrals of the regulators must be themselves *finite* calculable numbers. This is achieved by constructing functions of the scalar propagators whose singularities are integrated to zero in dimensional regularization, and then taking proper combinations of these objects.

We list the first few examples and their two-dimensional numerical values obtained from dimensional continuation

$$\frac{1}{(p^2)^2} \to K_{2,0} \equiv \frac{1}{(\hat{p}^2)^2} - \frac{1}{6}\frac{\hat{p}^4}{(\hat{p}^2)^3} \to -\frac{1}{96\pi},$$

$$\frac{1}{(p^2)^3} \to K_{3,0} \equiv \frac{1}{(\hat{p}^2)^3} - \frac{1}{4}\frac{\hat{p}^4}{(\hat{p}^2)^4} - \frac{1}{30}\frac{\hat{p}^6}{(\hat{p}^2)^4} + \frac{1}{24}\frac{(\hat{p}^4)^2}{(\hat{p}^2)^5} \to -\frac{7}{30720\pi},$$

$$\frac{\sum_\mu p_\mu^4}{(p^2)^4} \to K_{4,2} \equiv \frac{\hat{p}^4}{(\hat{p}^2)^4} + \frac{1}{6}\frac{\hat{p}^6}{(\hat{p}^2)^4} - \frac{1}{3}\frac{(\hat{p}^4)^2}{(\hat{p}^2)^5} \to -\frac{1}{128\pi},$$

$$\frac{\sum_\mu p_\mu^4}{(p^2)^5} \to K_{5,2} \equiv \frac{\hat{p}^4}{(\hat{p}^2)^5} + \frac{1}{6}\frac{\hat{p}^6}{(\hat{p}^2)^5} + \frac{7}{240}\frac{\hat{p}^8}{(\hat{p}^2)^5} + \frac{5}{12}\frac{(\hat{p}^4)^2}{(\hat{p}^2)^6}$$

$$- \frac{1}{8}\frac{\hat{p}^4\hat{p}^6}{(\hat{p}^2)^6} + \frac{5}{48}\frac{(\hat{p}^4)^3}{(\hat{p}^2)^7} \to -\frac{119}{737280\pi}, \tag{B.20}$$

where $\hat{p}^n = \sum_\mu \hat{p}_\mu^n$. As a consequence, the integrable singularities

$$\frac{P_{4,1}(p)}{(p^2)^4}, \qquad \frac{P_{4,1}(p)}{(p^2)^5}, \tag{B.21}$$

can be regulated by

$$4K_{4,2} - 3K_{2,0}, \qquad 4K_{5,2} - 3K_{3,0} - \frac{7}{184320\pi}, \tag{B.22}$$

respectively.

The last essential ingredient of computation is the evaluation of the lattice angular integrals in d dimensions (the continuum angular integrals are straightforward).

In computations $O(a^4)$, the general form of these integrals is

$$\int \frac{d^d p}{(2\pi)^d} \sum_{\mu\nu\rho\sigma} T_{\mu\nu\rho\sigma} k^\mu k^\nu k^\rho k^\sigma$$

$$= \frac{1}{d} \int \frac{d^d p}{(2\pi)^d} \left(\sum_\mu T_{\mu\mu\mu\mu} \right) \sum_\mu k_\mu^4$$

$$+ \frac{1}{d(d-1)} \int \frac{d^d p}{(2\pi)^d} \left[\sum_{\mu\nu} (T_{\mu\nu\mu\nu} + T_{\nu\mu\nu\mu} + T_{\mu\mu\nu\nu}) - 3 \sum_\mu T_{\mu\mu\mu\mu} \right]$$

$$\times \left[(k^2)^2 - \sum_\mu k_\mu^4 \right]. \tag{B.23}$$

We can now compute the cumulative contribution of the continuum integral and the lattice integral over the regulators of the IR singularities for the $O(a^4)$ expansion of $\Pi_0(k)$. The result, showing the cancellation of singularities (as expected) and allowing for the determination of $\Delta'_{4,l}$, is

$$\frac{1}{2\pi} \ln\left(\frac{k^2 a^2}{32} \right) + \frac{a^4}{48\pi} \left[P_{4,0} + \left(\tfrac{1}{2} \ln\left(\frac{k^2 a^2}{32} \right) - \tfrac{1}{3} \right) P_{4,1} \right], \tag{B.24}$$

and it implies

$$\Delta'_{4,0} = 0, \qquad \Delta'_{4,1} = \frac{1}{96\pi}. \tag{B.25}$$

Numerical integration of the regulated integrals leads to the following results (for $r_2 = \frac{1}{3}$)

$$\Delta_2 = 0.00674267, \qquad \Delta_{4,0} = 0.004746, \qquad \Delta_{4,1} = 0.002334. \tag{B.26}$$

More generally, the values of Δ_2, $\Delta_{4,0}$ and $\Delta_{4,1}$ as functions of $r = 3r_2$ are plotted in fig. 21.

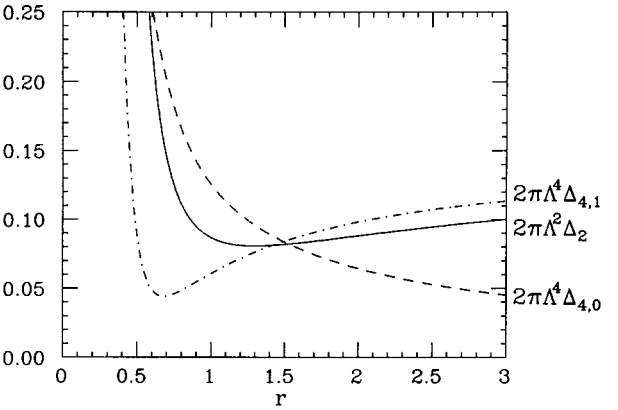

Fig. 21. The coefficients Δ_2, $\Delta_{4,0}$ and $\Delta_{4,1}$ in natural units for eq. (A.8), as functions of $r = 3r_2$.

The agreement of the truncated series with the numerical value of $\Pi_0(k)$ is remarkably good in the region $k \leqslant \Lambda$. This implies an estimate for the coefficients $\Delta_{6,l}$ which is consistent with an effective convergence radius O(1) in the variable k^2/Λ^2.

References

[1] G. Parisi, Les Houches lectures 1985 (North Holland, Amsterdam, 1987) and references therein.
[2] I. Montvay, Rev. Mod. Phys. 59 (1987) 263, and references therein.
[3] G. Parisi and Y.-S. Wu, Sci. Sin. 24 (1981) 483
[4] G. Parisi, Nucl. Phys. B180 [FS2] (1981) 378; B205 [FS5] (1982) 337
[5] G.G. Batrouni, G.R. Katz, A.S. Kronfeld, G.P. Lepage, B. Svetitsky and K.G. Wilson, Phys. Rev. D32 (1985) 2736
[6] R. Gavai and M. Creutz, Nucl. Phys. B280 [FS18] (1987) 181
[7] F. Fucito, E. Marinari, G. Parisi and C. Rebbi, Nucl. Phys. B180 [FS2] (1981) 369
[8] F. Fucito and E. Marinari, Nucl. Phys. B190 [FS3] (1981) 266
[9] H. Hamber, E. Marinari, G. Parisi and C. Rebbi, Phys. Lett. B124 (1983) 99; Nucl. Phys. B225 [FS9] (1983) 475
[10] P. de Forcrand and I.O. Stematescu, Nucl. Phys. B261 (1985) 613
[11] R.V. Gavai, A. Gocksch and U.M. Heller, Nucl. Phys. B283 (1987) 381
[12] M. Fukugita, Y. Oyanagi and A. Ukawa, Nucl. Phys. B291 (1987) 164
[13] R.V. Gavai, J. Potvin and S. Sanielievici, Phys. Lett. B183 (1987) 86
[14] D.J. Gross and A. Neveu, Phys. Rev. D10 (1974) 3235
[15] J.F. Schonfeld, Nucl. Phys. B95 (1975) 148
[16] R.G. Root, Phys. Rev. D11 (1975) 831
[17] P.P. Kulish and N. Yu. Reshetikin, Sov. Phys. JETP 53 (1981) 108
[18] R.F. Dashen, B. Hasslacher and A. Neveu, Phys. Rev. D12 (1975) 2443
[19] E. Witten, Nucl. Phys. B142 (1978) 285
[20] A. Zamolodchikov and A.B. Zamolodchikov, Phys. Lett. B72 (1978) 481
[21] M. Karowsky and H.J. Thun, Nucl. Phys. B190 [FS3] (1981) 61
[22] K.G. Wilson, *in* New phenomena in subnuclear physics, ed. A. Zichichi (Erice, 1975) (Plenum, New York, 1977)

[23] F. David and H.W. Hamber, Nucl. Phys. B248 (1984) 381
[24] K. Symanzik, *in* Mathematical problems in theoretical physics, Lecture notes in physics 153, ed. R. Schrader et al. (Springer, Berlin, 1983)
[25] W. Wetzel, Nucl. Phys. B255 (1985) 659
[26] J. Polony and H.W. Wyld, Phys. Rev. Lett. 51 (1983) 2257
[27] S. Duane, Nucl. Phys. B257 [FS14] (1985) 652
[28] S. Duane and J. Kogut, Phys. Rev. Lett. 55 (1985) 2774
[29] R.V. Gavai, Nucl. Phys. B269 (1986) 530
[30] W. Wetzel, Phys. Lett. B153 (1985) 297
[31] F. Guerin and R.D. Kenway, Nucl. Phys. B176 (1980) 168
[32] Y. Cohen, S. Elitzur and E. Rabinovici, Phys. Lett. B104 (1981) 289; Nucl. Phys. B220 [FS8] (1983) 102
[33] I.K. Affleck, Phys. Lett. B109 (1982) 307
[34] G. Curci and G. Veneziano, Nucl. Phys. B292 (1987) 555